Probing Heme Protein Conformational Equilibration Rates with Kinetic Selection[†]

Wei Dong Tian, J. Timothy Sage, and Paul M. Champion*

Department of Physics and Center for Interdisciplinary Research on Complex Systems, Northeastern University, Boston, Massachusetts 02115

Ellen Chien and Stephen G. Sligar

Department of Biochemistry and Chemistry, University of Illinois, Urbana, Illinois 61801

Received October 17, 1995; Revised Manuscript Received December 20, 1995[⊗]

ABSTRACT: Double-pulse flash photolysis experiments on solutions of carbonmonoxymyoglobin (MbCO) are used to determine the time scale for protein conformational averaging. The interconversion times for transitions between the "open" and "closed" subpopulations of MbCO are found to be $10^{-6}-10^{-4}$ s, depending on solvent composition and temperature. In aqueous solution at 273 K, the interconversion rate is found to be 1.4×10^6 s. Since the interconversion rate is comparable to or slower than the geminate rebinding rate, we describe the geminate phase of the kinetics as a superposition of contributions from the open and closed states. Although geminate kinetics remain intrinsically nonexponential for both open and closed states near room temperature, we find that substates within these two subpopulations interconvert more rapidly than the geminate rebinding. These observations cannot be explained by a superposition of contributions from a quasicontinuous conformational distribution (Steinbach et al., 1991) and are probably due to the long-time tail of the relaxation of the protein (Tian et al., 1992). Bimolecular rebinding takes place at a statistically averaged rate, since the interconversion and relaxation rates are faster than the bimolecular kinetics. The geminate and bimolecular kinetics are analyzed quantitatively as a function of pH using this approach and the spectroscopically determined populations of the open and closed states. The analysis accounts for the observed kinetics and also successfully predicts the kinetic response observed in the double-pulse experiments. In aqueous solution at 273 K, the geminate amplitudes and rates are found to be $I_g^0 = 32\%$ and $k_g^0 = 1.3 \times 10^7$ s^{-1} for the open state and $I_g^1 = 9.3\%$ and $k_g^1 = 1.4 \times 10^6$ s^{-1} for the closed state. In 75% glycerol solution at 264 K, the dominant component of the geminate rebinding is characterized by $I_{g1}^0 = 89\%$ and $k_{g1}^0 = 3.1 \times 10^6$ s^{-1} for the open state and $I_{g1}^1 = 26\%$ and $k_{g1}^1 = 3.1 \times 10^6$ s^{-1} for the closed state. The fact that the interconversion rate is comparable to the geminate rate of the closed state in aqueous solution is consistent with the idea that the open state provides an important pathway for ligand escape from (or entry to) the heme pocket (Tian et al., 1993). The increased viscosity of 75% glycerol solution delays the closed → open interconversion until the end of the geminate phase, which forces the ligand to find alternative pathways to the solution. This observation, in conjunction with the near equivalence of the geminate rates for the open and closed states in 75% glycerol solution, suggests that the solvent composition fundamentally alters the protein−ligand dynamics.

Myoglobin (Mb) plays a key physiological role in the reversible binding and storage of dioxygen. It is also one of the simplest heme proteins and has been studied extensively using a variety of physical techniques (Sage & Champion, 1996). The heme group in Mb is embedded in the protein matrix and covalently linked to the protein through the proximal histidine. The central iron atom reversibly binds small ligands such as dioxygen (O_2) and carbon monoxide (CO) at the sixth coordination site on the distal side of the heme. In the deoxy state, the ferrous iron atom is high-spin ($S = 2$) and switches to low-spin ($S = 0$) in the ligand-bound state. The different electronic structures associated with the heme group of ligated and deligated Mb allow changes on its optical properties to be used as a convenient method for observing ligand binding in flash photolysis kinetics experiments.

The kinetics of MbCO[1] have been studied over wide ranges of time and temperature by flash photolysis experiments (Gibson et al., 1956, 1986; Antonini & Brunori, 1971; Austin et al., 1975; Doster et al., 1982; Henry et al., 1983; Ansari et al., 1987, 1992; Olson et al., 1988; Lambright et al., 1991; Steinbach, et al., 1991; Tian et al., 1992, 1993). At low temperature ($T < 180$ K), the ensemble is "frozen", so that many different noninterconverting protein conformations are present (quenched disorder) and the barriers for ligand escape from the heme pocket become high enough that geminate recombination dominates the kinetic response. Under these conditions, the system is clearly characterized by a distribution of rebinding rates (Austin et al., 1975). It has been shown that a distribution of iron out-of-plane equilibrium positions can account quantitatively for the low-temperature kinetic data as well as for a variety of other experimental observations (Šrajer et al., 1988; Champion, 1987, 1992; Šrajer & Champion, 1991; Sage & Champion, 1996). The mean out-of-plane position at low temperature (a_0^*) was found to be ∼ 0.2 Å (Šrajer & Champion, 1991),

[†] This work was supported by NSF 94-05979 and NIH AM-35090.
[⊗] Abstract published in *Advance ACS Abstracts,* February 15, 1996.

[1] Abbreviations: MbCO, carbonmonoxymyoglobin; YAG, yttrium−aluminum−garnet; CW, continuous wave; H64L, bacterially expressed mutant Mb with His64 replaced by Leu.

0006-2960/96/0435-3487$12.00/0

which is intermediate between the bound (in-plane) and fully relaxed states ($a_0 \sim 0.45$ Å). Above the transition temperature ($T_g \sim 185$ K), the protein is free to relax to its deoxy conformation after photolysis and the ligand begins to escape to the solvent.

The conformational energy landscape of MbCO has been described using a tier concept (Frauenfelder et al., 1990, 1991; Young et al., 1991). The states of tier 0 include three primary conformations, A_0, A_1, and A_3, identified with CO vibrational frequencies near 1966, 1945, and 1933 cm^{-1}, respectively (Caughey et al., 1981; Ansari et al., 1987). These states have been assigned to "open" (A_0) and "closed" ($A_1 + A_3$) conformations of the distal pocket (Morikis et al., 1989). Within the states associated with "tier 0", the protein can assume a large number of substates of "tier 1", separated by smaller barriers. As discussed previously (Šrajer et al., 1986, 1988), protein conformations that lead to a distribution of heme iron displacements in the unbound state are likely to be of primary importance for an explanation of the nonexponential geminate rebinding at $T < 160$ K, and we suggest that these conformations are good candidates for functionally important tier 1 substates. The functional significance of additional distal pocket conformational changes within tier 1 and putative lower tiers (Frauenfelder et al., 1990) are less clear.

The presence of multiple thermally accessible conformations can be an important influence on both spectroscopic and kinetic measurements, which ordinarily represent an average over a large number of molecules. In some cases, it is possible to understand an experimental observation (such as a spectral band shape or rebinding curve) as a superposition of distinct contributions from individual conformations, and the sample is described as "inhomogeneous". A necessary condition for this situation is an observational time scale faster than the rate of conformational interconversion. On the other hand, when conformational interconversion is sufficiently rapid, each protein in the ensemble samples the full range of thermally accessible conformations on the observational time scale and contributes identically to the experimental observable. Since this is experimentally indistinguishable from a situation with all proteins in exactly the same conformation, the ensemble is often described as "homogeneous" in this case. However, it must be borne in mind that this description depends as much on the experimental probe used as on the sample.

The "homogeneous" vs "inhomogeneous" terminology begins to become cumbersome when conformational interconversion takes place on a wide range of time scales. For example, since tier 0 will have the slowest interconversion time, due to the larger barriers associated with the transitions between the open and closed states of the distal pocket, there will be time scales on which tiers 1 and 2 are "homogeneous", but tier 0 remains "inhomogeneous" (Tian et al., 1992). Similarly, the wide time range over which ligand rebinding occurs may lead one to speak of a transition from "inhomogeneous" to "homogeneous" behavior in the course of a single rebinding curve (Agmon et al., 1994). Where possible, it is preferable to refer to a quantitative measurement of the rate of conformational equilibration.

A topical example of the importance of conformational interconversion times involves the kinetic analysis of MbCO and its nonexponential geminate recombination. Nonexponential geminate recombination has been observed both at low temperature (Austin et al., 1975) and at room temperature (Lambright et al., 1991; Tian et al., 1992; Ansari et al., 1992). At low temperature ($T < 160$ K), the nonexponential rebinding kinetics are described using a distribution of activation enthalpies, $g(H_{BA})$, which reflect a "frozen", noninterconverting distribution of conformational substates. On the other hand, no consensus exists regarding the origin of the nonexponential kinetic behavior near room temperature. It has been variously attributed to MbCO distal (Tian et al., 1992) and proximal (Ansari et al., 1992) relaxation processes as well as to residual effects of conformational inhomogeneity, associated with a fraction of the most rapidly binding substates (Steinbach et al., 1991). In this paper, we use double-pulse kinetic experiments to probe the rate of interconversion among tier 0 and tier 1 substates and to explain the pH dependence of the MbCO geminate rebinding kinetics.

When CO is complexed to Mb, the FeCO vibrations associated with tier 0 can be observed by both resonance Raman (Kerr & Yu, 1988; Morikis et al., 1989) and infrared (Caughey et al., 1981; Alben et al., 1982; Ansari et al., 1987) spectroscopy. As mentioned above, the A_0, A_1, and A_3 states have also been assigned using pH and site-directed mutation studies (Morikis et al., 1989) to "open" (A_0) and "closed" (A_1, A_3) distal pocket conformational states. The open- and closed-state populations are a function of pH and have been correlated with protonation of the distal histidine in native MbCO (Morikis et al., 1989). These assignments have been confirmed by X-ray (Quillin et al., 1992) and single-crystal Raman (Zhu et al., 1992) studies, which show that as the pH is lowered, the distal histidine swings away toward the more polar environment of the solvent, where it is protonated. This displacement of the distal histidine, also observed on binding bulky ligands (Ringe et al., 1984), has been proposed to open a pathway for ligand exit from and entry to the active site (Perutz & Mathews, 1966; Chance et al., 1966; Case & Karplus, 1979; Johnson et al., 1989). Since the open and closed population can be controlled by varying pH, Raman and IR spectra can be used as a direct measure of these populations in order to analyze the pH-dependent kinetic response (Tian et al., 1993). At very low pH (<4.0), the protein partially unfolds and the iron−histidine bond breaks in metMb and deoxyMb, while in MbCO the bond remains intact until the pH reaches 2.6 (Sage et al., 1991a,b). This global pH-dependent conformational change is clearly distinguished from the more localized changes upon conversion from the open to the closed state (Morikis et al., 1989). In the present study the pH is kept above 4.4, so that the unfolding process does not affect the ligand binding kinetics.

In previous work (Tian et al., 1993), we analyzed the ligand association and dissociation rates of myoglobin as a function of pH in aqueous solution and showed that the interconversion between the open and closed states is relatively fast (∼1−10 μs) compared to these rates. As a result, those rates can be treated by averaging over the open and closed populations. In aqueous solution between 273 and 293 K, the association (k_{on}^0) and dissociation (k_{off}^0) rates of the open state of MbCO are about an order of magnitude larger than for the closed state (Tian et al., 1993). This suggests that the open state plays a physiologically relevant role even though it comprises only ∼5% of the time-averaged

population at pH 7. An even more dramatic increase ($\sim 10^3$) in the dissociation rate of the open form of MbO_2 was also observed and assigned to the loss of the hydrogen bond between O_2 and the distal histidine, which stabilizes the bound O_2 in the closed form. We have suggested that the transition from the closed to open conformation in MbO_2 may have physiological relevance for the control of oxygen release in muscle cells (Tian et al., 1993).

Here, we extend our consideration of the data to include the geminate phase of recombination and use a population-weighted superposition analysis to independently characterize the kinetic properties of the open and closed states. More importantly, this analysis provides a quantitative determination of the rate of interconversion between open and closed states. This information is essential to evaluate the hypothesis that the transition from the closed to the open state facilitates ligand exit from and entry to the binding pocket.

EXPERIMENTAL PROCEDURES

Many of the sample preparation and the experimental protocols (e.g., Raman spectroscopy, flash photolysis, association and dissociation kinetics) have been presented elsewhere (Tian et al., 1992, 1993; Morikis et al., 1989; Zhu et al., 1992). Native sperm whale metMb in lyophilized form was obtained from Sigma Chemical Co. Mb samples were prepared in a 0.1 M/0.2 M citrate/phosphate buffer solution for the pH-dependent measurements. Solvents included aqueous buffers and mixtures with glycerol (35% and 75% by volume). A myoglobin mutant sample H64L was expressed from a synthetic gene in *Escherichia coli* as previously described (Springer & Sligar, 1987) and prepared in a phosphate buffer (0.1 M) at pH 7. All the samples were degassed with a stream of N_2, reduced with a 20-fold excess of dithionite, and saturated with CO. Due to the high viscosity of glycerol, a longer time is needed to degas the sample (30−60 min) and saturate CO in the solution (10−20 min) than for aqueous solution. All pH values were obtained using a Beckman Instruments Φ 40 pH meter after addition of Mb to the buffer solution. The pH and optical spectra were measured before and after the kinetics experiments to verify that no changes had occurred. The difference in OD between the equilibrium deoxyMb and MbCO samples at the monitoring wavelength (ΔA_{eq}) was used to normalize the CO rebinding kinetics.[2]

A 10-Hz Nd-doped yttrium−aluminum−garnet (YAG) laser generates 10-ns pulses at 532 nm that photolyze the solution sample of MbCO. The intensity is adjusted by an attenuator to a level (10−20 mJ/pulse) that just maximizes the change in transmission, ensuring that the sample is totally photolyzed (≥98%) with a minimum heating effect. The attenuated beam from a tunable CW dye laser ($\sim 20\ \mu W$) is used to monitor the kinetic response of the sample at selected wavelengths. The polarization of the pump and probe beams are scrambled using quartz wedges to eliminate the linear dichroism contribution to the ligand rebinding signal from the relatively slow (≥100 ns) rotational diffusion of the protein in glycerol solution (Ansari et al., 1993). The signal is detected by a high-linearity low-noise photomultiplier tube (R955 Hamamatsu with HC123-01 high-voltage supply and divider) operated at 600 V and averaged using a 350-MHz digital oscilloscope (LeCroy 9420). The signal is averaged about 5×10^3 times to reduce random noise, and the YAG laser is grounded spearately and shielded in order to reduce radiofrequency (rf) noise. A background signal recorded with the probe beam blocked is used to correct for the offset of the oscilloscope and for residual rf noise.

Since ligand rebinding kinetics of myoglobin at room temperature can be observed over many decades (10^{-8}−10^{-1} s) and the oscilloscope covers only 4.5 decades with 10-ns resolution, two measurements of different time regions are needed to complete the experiment. The resulting digital voltage signals from the oscilloscope are transferred to a computer and converted into the absorbance change [$\Delta A(t)$] between the ligand-bound and photolyzed samples. The two sets of $\Delta A(t)$ are then logarithmically averaged and combined into one data set containing ~150 data points.

In the double-pulse experiments, the second pulse follows the first pulse after a delay time τ and rephotolyzes the fraction of the ensemble that has bound ligand between pulses. The difference between the kinetic response of a single- and a double-pulse experiment that is suitably normalized reveals the kinetics of the proteins that have rebound ligand during the time τ (see Theory). A beam splitter and a set of prisms are used to generate optical delays up to 100 ns. For longer delays, the YAG laser is synchronized and a digital delay/pulse generator (DG535, Stanford Research System, Inc.) is used to trigger an excimer laser (EMG 53MSC, Lambda Physics) after the designated delay time. The excimer laser pumps a dye laser (Lumonics HyperDYE-300) and creates 10-ns photolysis pulses at 581 nm (the peak of rhodamine 6G). The two pump beams are focused and overlapped with the probe beam throughout the sample. Care is taken to adjust the photolyzing pulse energy and beam diameters to completely photolyze the interaction volume (≥98% photolysis with the first pulse). The typical energy density is 500 mJ/cm^2 for the YAG pulse and 60 mJ/cm^2 for the excimer pulse. When the kinetics of the double-pulse and single-pulse experiments are compared, the total pump power is adjusted to be the same so that differential heating effects are avoided. The bimolecular rates of the single-pulse and the double-pulse experiments were compared and used to estimate that differential heating was less than 0.3 K.

In the double-pulse experiments, the first pulse completely photolyzed the ensemble (>98%), while under some circumstances, the second pulse did not achieve complete rephotolysis. In order to test for the possibility of conformationally specific photolysis, a control experiment was performed by varying the intensity of the second pulse (Tian, 1995b). When the average power was changed from 10 to 200 mW (~20−100% photolysis), the normalized kinetics did not show any difference within the error, indicating that the photolysis yield is independent of the functionally important conformational states in MbCO. As a result, eq 13b and 14b (see below) can be used to analyze the CO rebinding kinetics of myoglobin, under the condition of incomplete photolysis in the second pulse.

The optimal wavelength for monitoring the MbCO rebinding kinetics was found to be 423 nm, which maximizes the detected transmission change at short times. A comparison between the absorption change at the first time point in the kinetics measurement, ΔA (10 ns), with ΔA_{eq} from the

[2] ΔA_{eq} is temperature-dependent due to changes in the deoxyMb and MbCO absorption with temperature; ΔA_{eq} changes ~0.4%/K.

equilibrium measurement of deoxy and MbCO shows very good agreement (±1%) for samples in pH 7 aqueous solution at 293 K. In 75% glycerol solutions ΔA (10 ns) is too large by about 3%, presumably due to the fact that the deoxyMb absorption spectrum has not yet reached equilibrium and is slightly red-shifted with respect to the equilibrium species (Lambright et al., 1991; Tian et al., 1992; Ansari et al., 1992). In order to further examine the influence of spectral relaxation on the CO rebinding kinetics, measurements were also made at the equilibrium isosbestic point of the deoxy and MbCO absorption bands. The monitoring wavelength was adjusted to approximately 429.5 nm (the isosbestic point shifts with different temperature and solution conditions) and tuned to make the beginning of the bimolecular phase disappear. The kinetics measured at this wavelength monitor the time evolution of the photoproduct Soret band (Tian et al., 1992).

THEORY

(A) General Considerations. We describe the normalized rebinding kinetics $N(t)$ following ligand photolysis as the ratio

$$N(t) = \frac{\Delta A(t)}{\Delta A_{\max}} \tag{1}$$

of the transient absorbance signal $\Delta A(t)$ to the total absorbance change $\Delta A_{\max}$ that would take place upon complete deligation of the sample.[3] A kinetic selection experiment consists of comparing the ligand rebinding kinetics $N_D(t; \tau)$ of a sample exposed to two photolyzing pulses applied at $t = 0$ and at $t = \tau$ to the kinetics $N_S(t)$ observed under the same conditions, but with the second pulse blocked (see Figure 1, left panel). For the present, we assume that all proteins in the sample are photolyzed by each of the pulses, so that $N_D(0; \tau) = 1$, $N_D(\tau; \tau) = 1$, and $N_S(0) = 1$, and we define the quantity

$$N^*(t, \tau) = \frac{N_D(t + \tau; \tau) - N_S(t + \tau)}{1 - N_S(\tau)} \tag{2}$$

which describes the renormalized kinetics of molecules that rebind during the delay time τ. The normalization factor in the denominator of eq 2 ensures that $N^*(0, \tau) = 1$ and facilitates comparison to the kinetics, $N_S(t)$, of the full ensemble. When a sample contains a distribution of kinetically distinct molecules, $N^*(t, \tau)$ describes a "kinetically selected" subpopulation of the full ensemble with a disproportionate contribution of faster rebinding molecules. On the other hand, for a "homogeneous" sample, all the conformations average prior to arrival of the second pulse and

$$N^*(t, \tau) = N_S(t) \tag{3}$$

[3] $\Delta A_{\max}$ is the true absorbance change at $t = 0$ after complete photolysis. In the actual analysis, this value can be only estimated due to the time resolution of the instruments. Therefore, we use the equilibrium absorbance change between MbCO and deoxyMb, ΔA_{eq}, to normalize the data. The small increase of $\Delta A_{\max}$ compared to ΔA_{eq} may be due to incomplete protein relaxation which generates a slightly red-shifted Mb* Soret absorption band at early times after photolysis (Lambright et al., 1991; Tian et al., 1992; Ansari et al., 1992.).

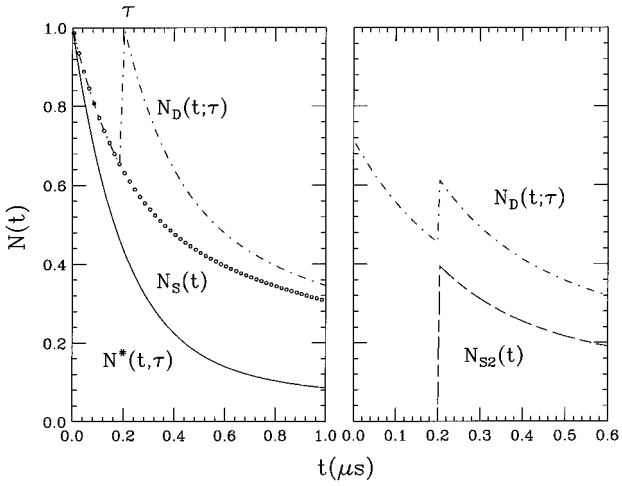

FIGURE 1: (Left panel) Theoretical double-pulse experiment for complete photolysis. The open circles represent the single-pulse kinetics $N_S(t)$. The dash−dotted line represents the double-pulse kinetics $N_D(t, \tau)$, where a second pulse rephotolyzes the ensemble after a delay time τ. The solid line is the normalized difference kinetics $N^*(t, \tau)$ of the rephotolyzed subpopulation, defined by eq 2. (Right panel) A variation of the double-pulse experiment useful under conditions of incomplete photolysis. The dashed line represents the single-pulse kinetics, $N_{S2}(t)$, where photolysis is carried out by the second pulse alone (the first pulse is blocked). The dash−dotted line represents the double-pulse kinetics, $N_D(t, \tau)$.

Strictly speaking, of course, even pure molecular ensembles are inhomogeneous in a condensed phase if probed on sufficiently rapid time scales, due to the existence of multiple conformations and variations in local environment. However, if each molecule samples all thermally accessible conformations before the second pulse arrives, the molecular subpopulation photolyzed by the second pulse will contain the same distribution of conformations as the full ensemble in equilibrium. Measurements of $N^*(t, \tau)$ as a function of the delay time τ thus contain information about conformational interconversion rates.

To extract this information in a more quantitative way, consider the (experimentally unrealizable) case in which, immediately before photolysis, the entire ensemble is in a nonequilibrium state with all molecules in the same (ith) conformation. The resulting survival fraction $N_i(t)$ will be affected not only by rebinding to molecules in conformation i but also by the population of kinetically distinct conformations $j \neq i$ as the ensemble relaxes and equilibrates at longer times. The rate of rebinding to conformation i determines $N_i(t)$ at short times. At longer times, $N_i(t)$ will also be affected by the rate, λ, of equilibration with other conformations $j \neq i$ and the rates of rebinding to these conformations. At times $\lambda t \gg 1$, the kinetics will be determined by the equilibrium distribution of conformations, independent of the initial conditions.

Note that the kinetics $N_{i\gamma}(t)$ observed for individual molecules, γ, in the conformation i may differ, due to varying ligand trajectories. The kinetics associated with molecules in the ith conformation, $N_i(t) \equiv \langle N_{i\gamma}(t) \rangle_\gamma$, arises from an average over all molecules in that conformation. Thus, a conformationally homogeneous ensemble will meet the criterion defined by eq 3, even if the ligand trajectories vary among individual molecules and lead to nonexponential kinetics.

In the general case, the ensemble prior to photolysis will include a number of conformations in thermal equilibrium with populations P_i (normalized so that $\sum_i P_i = 1$). However, if the ensemble kinetics (conformational interconversion as well as ligand diffusion and rebinding) are described by any set of linear differential equations (which may include diffusion as well as reaction kinetics), we can express the rebinding kinetics

$$N_S(t) = \sum_i P_i N_i(t) \tag{4}$$

of the full ensemble as a superposition of the functions $N_i(t)$ defined above, weighted by the initial equilibrium populations P_i. In contrast, the kinetics

$$N^*(t, \tau) = \sum_i P_i^*(\tau) N_i(t) \tag{5}$$

of the kinetically selected subensemble are determined by the fraction $P_i^*(\tau)$ of rebound molecules found in conformation i just prior to the second pulse, which will, in general, differ from the equilibrium populations P_i. For example, in the case that the rate, λ, of conformational equilibration is so slow that little interconversion takes place during the delay time τ, then

$$P_i^*(\lambda\tau \ll 1) = \frac{P_i[1 - N_i(\tau)]}{\sum_i P_i[1 - N_i(\tau)]} = \left[1 - \frac{N_i(\tau) - N_S(\tau)}{1 - N_S(\tau)}\right] P_i \tag{6a}$$

As expected, conformations rebinding faster than the average $[N_i(\tau) < N_S(\tau)]$ are more strongly represented ($P_i^* > P_i$) in the kinetically selected subpopulation than in the full molecular ensemble, since the second pulse only photolyzes molecules which rebind within the delay time τ. In the opposite limit of rapid conformational interconversion, the normalized populations

$$P_i^*(\lambda\tau \gg 1) = P_i \tag{6b}$$

in the kinetically selected subensemble have time to relax to the equilibrium values found in the full ensemble. In this limit, the kinetics described by eq 5 are identical to those of the full ensemble described by eq 4, and the system satisfies eq 3. The transition of the kinetically selected rebinding (eq 5) between the two limiting cases of eq 6a,b as τ is varied provides direct information on the rate, λ, of conformational equilibration.

If a distribution of conformations (with differing kinetics) exists, it is always possible to find a delay at short enough time scales so that $N^*(\tau)$ calculated from eqs 4, 5, and 6a will fail to satisfy eq 3. However, measurements at variable time delay are in general required to exclude certain hypothetical situations which may fortuitously satisfy the condition in eq 3. A trivial example cited by Nienhaus et al. (1994) involves biphasic rebinding, $N_i(t) = (1 - x)e^{-k_i t} + xe^{-k_i' t}$, in which the rates k_i and k_i' but not the amplitudes $(1 - x)$ and x of the fast and slow phases depend on molecular conformation. (This might occur in Mb, for example, if only the equilibrium B-state free energies were affected by conformational changes.) This "inhomogeneous" ensemble will satisfy eq 3 if the second pulse falls between two well-separated phases, even if conformational exchange is slow ($\lambda\tau \ll 1$). In this case, $k_i\tau \gg 1 \gg k_i'\tau$ for all i, so that $N_i(\tau) = x$ is independent of i and eq 6a yields $P_i^*(\tau) = P_i$. However, this hypothetical situation can be avoided by simply choosing a delay time that falls within one of the phases.

(B) Multiple-Pulse Sequence. Multiple-pulse experiments (Austin et al., 1975; Frauenfelder, 1983; Agmon et al., 1994) can also be used in certain situations to enhance the differences between the kinetically selected molecules and the full ensemble. Analogously to eq 2, we define the kinetics

$$N^{*(m)}(t, \tau) = \frac{N^{(m)}[t + (m-1)\tau] - N^{(m-1)}[t + (m-1)\tau]}{1 - N^{(m-1)}[(m-1)\tau]} \tag{7}$$

selected by the final pulse in a series of m pulses each separated by a delay τ as the normalized difference between the kinetics $N^{(m)}(t; \tau)$ observed in an m-pulse experiment and the kinetics $N^{(m-1)}(t; \tau)$ observed with the mth pulse blocked. The expression

$$N^{*(m)}(t) = \sum P_i^{*(m)} N_i(t) \tag{8}$$

analogous to eqs 4 and 5 still holds, and a generalization of the argument for the two-pulse case described above leads to

$$P_i^{*(m)}[(m-1)\lambda\tau \ll 1] = \frac{P_i - \sum_{n=1}^{m-1} P_i^{(n)} N_i[(m-n)\tau]}{1 - \sum_{n=1}^{m-1}\sum_i P_i^{(n)} N_i[(m-n)\tau]} \tag{9}$$

with $P_i^{(n)} = P_i - \sum_{l=1}^{n-1} P_i^{(l)} N_i[(n - l)\tau]$, the residual population in the ith conformation after n pulses. Equation 9 shows that the difference between $P_i^{*(m)}(\tau)$ and P_i increases with the number of pulses. For $m = 2$, this expression reduces to eq 6a.

(C) Direct Comparison between Single- and Double-Pulse Kinetics. In the limit of slow interconversion ($\lambda\tau \ll 1$), it is also possible to extract qualitative information about rebinding to individual members of the ensemble based on the comparison

$$N_D(t + \tau; \tau) = N_S(t) \tag{10}$$

of the kinetics after the first pulse to those after the second without subtraction and normalization as in eqs 2 and 3. This test is useful only under the assumption of a two-state system (i.e., only bound and geminate states) and has been used (Austin, et al., 1975; Frauenfelder, 1983) to establish the presence of a distribution of static molecular conformations within a low-temperature protein ensemble. The usefulness of this test can be explored if we use eqs 2, 4, 5, and 6a to express total kinetics observed following the second pulse ($t > 0$) in the limit of slow interconversion ($\lambda\tau \ll 1$) as

$$N_D(t + \tau; \tau) = N_S(t) + \sum_i P_i[N_i(t + \tau) - N_i(t)N_i(\tau)] \tag{11}$$

The condition of eq 10 can be met in this limit only by an ensemble of two-state systems having individual conformations which bind with single exponentials, so that $N_i(t + \tau) = N_i(t)N_i(\tau)$ for all i.

Strictly speaking, then, the condition of eq 10 does not test for "inhomogeneity" but rather for single-exponential rebinding to the individual conformations. The fact that heme protein geminate rebinding kinetics observed at low temperatures meet the condition in eq 10 demonstrates (Austin et al., 1975) that the highly nonexponential kinetics must arise from an ensemble of molecules with a broad distribution of exponential rebinding rates rather than from a "homogeneous" ensemble with nonexponential kinetics (e.g., due to multiple ligand rebinding trajectories within each conformation).

We emphasize that a failure to meet the condition in eq 10 may occur either in the limit $\lambda\tau \ll 1$, due to nonexponential rebinding to individual conformations, *or* in the limit $\lambda\tau \gg 1$, if $N_S(t)$ remains nonexponential. For example, even a "homogeneous" ensemble containing a single protein conformation may have a nonexponential $N_S(t)$ (for example, due to multiple rebinding trajectories) and thus fail to satisfy eq 10.[4] An inhomogeneous ensemble can also fail the test (eq 10), if the individual conformations rebind nonexponentially (e.g., if ligand escape occurs and rebinding is biexponential). As a result, eq 10 cannot be used to determine conformational transition rates, in contrast to eq 3, which always holds at sufficiently long delay times.

An example of the need for caution in using the test characterized by eq 10 is seen in recent work by Doster and co-workers (Post et al., 1993; Agmon et al., 1994), who report multiple-pulse experiments carried out on horse MbCO in pH 7 75% glycerol at 185 K. With a delay time $\tau = 0.1$ s, these workers observe deviations from eq 10 beginning at a time they define as t_{inhomog} and imply that conformational fluctuation begins on this time scale, i.e., $\lambda \simeq t_{inhomog}^{-1}$. If this interpretation were accepted, the appearance of these deviations at times on the order of 10^{-4} s would contradict earlier measurements (Young et al., 1991; Iben et al., 1989) that led to an estimated time scale $\simeq 10^2$ s for conformational fluctuation among substates of tier 1 at 185 K. However, as pointed out previously (Frauenfelder, 1983), deviations from eq 10 actually suggest optical pumping of long-lived states even in the inhomogeneous limit $\lambda\tau \ll 1$. For example, suppose that after photolysis there is a small probability x that the ligand, instead of rebinding to the heme at a rate k_i, migrates to another location in the protein from which it rebinds at a much slower rate k_i', so that rebinding to conformation i follows $N_i(t) = (1 - x)\exp(-k_i t) + x\exp(-k_i' t)$ (which is not the single exponential required to satisfy eq 10). In this case

$$N_i(t+\tau) - N_i(\tau)N_i(t) = x(1-x)[e^{-k'_i\tau} - e^{-k_i\tau}][e^{-k'_i t} - e^{-k_i t}] \quad (12)$$

in the inhomogeneous limit $\lambda\tau \ll 1$. Substitution into eq 11 shows that, relative to $N_S(t) = \sum_i P_i N_i(t)$, the slow phase of $N_D(t + \tau)$ increases by an amount $x(1 - x)[\exp(-k_i'\tau) - \exp(-k_i\tau)]$ at the expense of the fast phase. This expression shows that the size of this change will be largest when the second pulse falls between the phases, i.e., $k_i\tau > 1 > k_i'\tau$. The amplitude of the slow phase will continue to increase with the introduction of additional pulses (Frauenfelder, 1983). If such optical pumping is assumed, the results from Doster's laboratory are qualitatively consistent with an ensemble composed of multiple (>2) state systems exhibiting nonexponential (or multiple-exponential) rebinding, which do not interconvert on the experimental time scale.

(D) Incomplete Photolysis. In all of the above discussion, we have assumed that both pulses completely photolyze the sample. When complete photolysis is experimentally unattainable, the analysis of kinetic selection measurements requires additional care, since different conformations may be photolyzed by varying amounts. If a fraction $\phi_i^{(1)}$ of the molecules in conformation i are photolyzed by the first pulse, the kinetics follow the expression

$$N_S(t) = \sum_i P_i \phi_i^{(1)} N_i(t) \quad (13a)$$

in the absence of a second pulse. Note that $N_i(0) \equiv 1$ but that $N_S(0) < 1$ in the presence of conformations with $\phi_i^{(1)} < 1$. The difference kinetics

$$N^*(t, \tau) = \sum_i P_i^*(\tau)\phi_i^{(2)} N_i(t) \quad (14a)$$

defined by eq 2 are determined not only by the fraction $P_i^*(\tau)$ of the unphotolyzed sample in conformation i but also by the probability $\phi_i^{(2)}$ that a molecule in that conformation is photolyzed by the second pulse (in general, $\phi_i^{(2)} \neq \phi_i^{(1)}$, if pulse intensities are different).

The populations

$$P_i^*(\lambda\tau \ll 1) = \frac{P_i[1 - \phi_i^{(1)}N_i(\tau)]}{\sum_i P_i[1 - \phi_i^{(1)}N_i(\tau)]} = \left[1 - \frac{\phi_i^{(1)}N_i(\tau) - N_S(\tau)}{1 - N_S(\tau)}\right] P_i \quad (15)$$

appearing in eq 14a in the limit $\lambda\tau \ll 1$ are also altered due to incomplete photolysis by the first pulse. The decreased effectiveness of the selection of fast rebinding conformations due to the presence of the additional factor of $\phi_i^{(1)} < 1$ in eq 15 takes place because the fraction of the sample not photolyzed by the first pulse retains the equilibrium population distribution determined by P_i. The use of kinetic selection techniques thus requires better signal-to-noise in the case of incomplete photolysis. Caution is also required in the other limit, where $P_i^*(\lambda\tau \gg 1) = P_i$, as the resulting kinetics for conformationally specific photolysis

$$N^*(t; \lambda\tau \gg 1) = \sum_i P_i \phi_i^{(2)} N_i(t) \quad (16)$$

still differ from $N_S(t)$ (eq 13a) unless $\phi_i^{(2)} = \phi_i^{(1)}$. Thus, under conformationally specific photolysis conditions, the test (eq 3) for conformational homogeneity is valid only if the two photolyzing pulses are carefully adjusted to have equal intensity. A convenient alternative procedure under such conditions is to compare $N^*(t, \tau)$ with the single-pulse kinetics, $N_{S2}(t)$ recorded with the *first* pulse blocked, which automatically satisfies the equal photolysis condition (Figure 1, right panel).

It is also possible that incomplete photolysis can arise under conditions that are independent of conformation. This

[4] Such a system will satisfy eq 3, but substitution of eq 3 into eq 2 yields $N_D(t + \tau;\tau) = N_S(t) + [N_S(t + \tau) - N_S(t)N_S(\tau)]$ so that eq 10 holds only if $N_S(t)$ is exponential.

situation can be experimentally distinguished by varying the intensity of the pump pulse and comparing the ligand rebinding kinetics as a function of photolysis level (taking care to minimize heating effects). If the rescaled kinetics change with the intensity of the pump pulse, it indicates that ϕ is conformation-dependent. However, if the kinetics are independent of photolysis level, ϕ can be taken as independent of conformation, so that[5] $\phi_i^{(1)} = \phi^{(1)}$ and $\phi_i^{(2)} = \phi^{(2)}$. This means that eqs 13a and 14a become

$$N_S(t) = \phi^{(1)} \sum_i P_i N_i(t) \tag{13b}$$

and

$$N^*(t, \tau) = \phi^{(2)} \sum_i P_i^*(\tau) N_i(t) \tag{14b}$$

which satisfy the condition

$$N_S(t) = (\phi^{(1)}/\phi^{(2)}) N^*(t, \tau) \tag{17}$$

in the limit $P_i^*(\tau) \rightarrow P_i(\tau)$. Thus, eq 3 can be generalized to the case of (conformationally independent) incomplete photolysis by simply rescaling $N^*(t,\tau)$. (All the rebinding kinetics of MbCO discussed in this paper satisfy the condition that $\phi^{(1)}$ and $\phi^{(2)}$ are independent of conformation.)

RESULTS

One important issue concerning ligand binding to heme proteins at room temperature involves understanding whether protein conformational states interconvert slowly enough to contribute independently to the observed geminate recombination. The distal pocket mutant H64L is a good candidate for study, because it has a large geminate amplitude and, thus, a measured rate that directly reflects the binding of ligand to the heme, k_{BA}, rather than ligand escape, k_{out}. In addition, the H64L mutant lacks the discrete open and closed distal pocket states associated with native Mb (Balasubramanian et al., 1993). As a result, the slower interconversions between the "tier 0" substates (A_0, A_1, A_3) are not a major consideration and the experiment directly probes interconversion among the "tier 1" substates, which we assign to smaller-scale conformational fluctuations of the protein that induce changes in the heme geometry (Šrajer et al., 1988).

In Figure 2 we display the results of two-pulse kinetic selection measurements on the mutant H64L MbCO in 75% glycerol at 295 K with a delay time of 100 ns ($\phi_i^{(1)} = 1$, $\phi_i^{(2)} < 1$). The solid circles represent the normalized difference $N^*(t, \tau)$, between $N_D(t)$ (open diamonds) and $N_S(t)$ (open circles) from eq 2. We see that within experimental error $N_S(t) = N^*(t, \tau)/\phi^{(2)}$, indicating that at 295 K the conformational fluctuations associated with tier 1 take place much more rapidly than 100 ns under the experimental conditions of Figure 2.

Equation 3 tests for conformational equilibration ($P_i^*(\tau) \rightarrow P_i$) of the kinetically selected subensemble but does not directly demonstrate that *thermal* fluctuations are responsible. To test for the possibility (Chu et al., 1995) that absorption of additional photons following CO photolysis, rather than

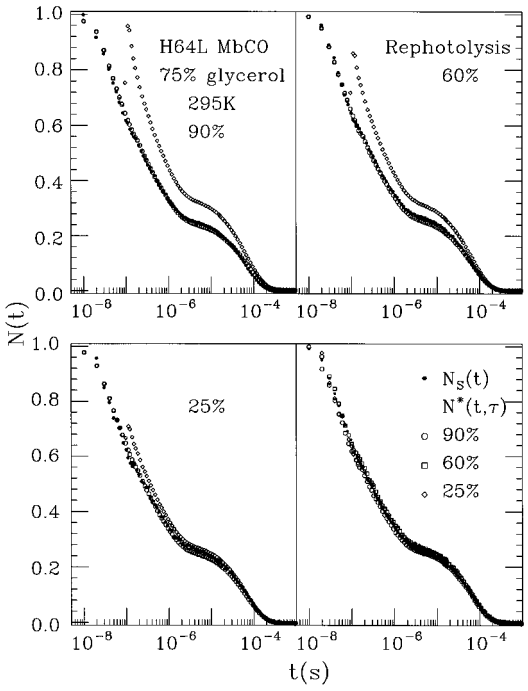

FIGURE 2: Double-pulse experiments of mutant H64L MbCO with differing amounts of the population rephotolyzed by the second pulse (τ = 100 ns). The sample was prepared at pH 7.0 in 75% glycerol solution at 295 K. The kinetics $N^*(t, \tau)$ of the rephotolyzed fraction that rebinds CO between the two pulses (solid circles) are extracted by subtracting the single-pulse kinetics $N_S(t)$ (open circles) from the double-pulse kinetics $N_D(t; \tau)$ (open diamonds) followed by renormalization and realignment of the time axis. Different rephotolysis percentages, 25%, 60%, and 90%, are obtained by varying the intensity of the second pulse. $N^*(t, \tau)$ is scaled by $C = 1/\phi^{(2)} = [1 - N_S(\tau)]/[N_D(\tau, \tau) - N_S(\tau)]$ for comparison. The scaling constants C are ~1.12, 1.62, and 4.05 for $N^*(t; \tau)$ with 90%, 60%, and 25% photolysis, respectively. The lower right panel presents the comparison of the kinetics of the whole ensemble to the kinetics with different rephotolyzed populations (after scaling).

thermal fluctuations, equilibrate the conformational distribution, we have verified that $N_S(t)$ does not vary with the pump intensity (Tian, 1995b). In addition, the measurements on H64L were repeated using variable intensity in the second pulse (Figure 2). When the intensity of the second pulse is reduced, incomplete rephotolysis leads to $N^*(\tau; \tau) < 1$, and eq 17 is used to renormalize $N^*(t, \tau)$ for comparison. The scaling factors $C = 1.12$, 1.62, and 4.05 represent the fraction photolyzed by the second pulse, $\phi^{(2)} = 90\%$, 60%, and 25%, respectively. The results (Figure 2) show that $CN^*(t, \tau) = N_S(t)$ even when only 25% of the rebound proteins are rephotolyzed by the second pulse. In this case, 80% of the proteins contributing to $N^*(t, \tau)$ absorb only a single photon from the second pulse,[6] so that multiple photon processes can be neglected. The lower right panel shows that the kinetic curves with differing rephotolyzed populations are identical within error to the kinetics of the full ensemble. This result, along with the intensity independence of the single-pulse experiments, demonstrates that thermal fluctuations, rather than photon-induced processes, are responsible

[5] $\phi^{(1)}$ can be estimated by $\Delta A(10\text{ ns})/\Delta A_{eq}$ and $\phi^{(2)}$ can be evaluated by $[N_D(\tau,\tau) - N_S(\tau)]/[1 - N_S(\tau)]$.

[6] We assume that absorptions of individual photons are independent events and write the probability of the heme to absorb n photons as $Q_n = Q_1^n$ for $n \geq 1$. The fraction of rebound material photolyzed by the second pulse at $t = \tau$ is $\phi^{(2)} = 1 - Q_0 = \sum_{n=1}^{\infty} Q_n = \sum_{n=1}^{\infty} (Q_1)^n = Q_1/(1 - Q_1)$. We can calculate the fraction of molecules photolyzed which absorb only a single photon from the second pulse as $Q_1/\phi^{(2)} = 1 - Q_1 = 1/(1 + \phi^{(2)})$.

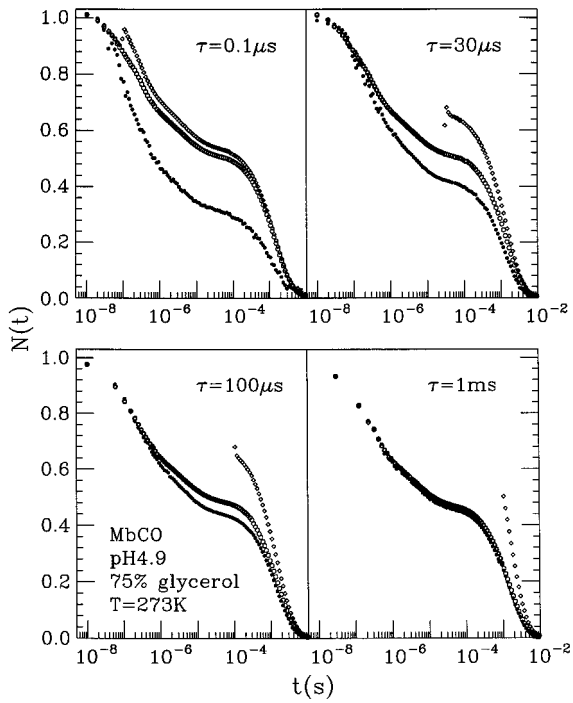

FIGURE 3: Double-pulse experiments on MbCO in pH 4.9 75% glycerol solution at 273 K with different delay times ($\tau = 0.1$ μs, 30 μs, 100 μs, and 1 ms). $N_S(t)$ (circles) and $N_D(t; \tau)$ (diamonds) are normalized with ΔA_{eq} obtained from equilibrium measurements. The kinetics of the rephotolyzed population, $N^*(t, \tau)$ (solid dots), were scaled by $C = 1/\phi^{(2)} = [1 - N_S(\tau)]/[N_D(\tau, \tau) - N_S(\tau)]$ for comparison. The scaling factors are 1.33, 1.47, 1.33, and 1.41 for delay times 0.1 μs, 30 μs, 100 μs, and 1 ms, respectively. It should be noted that the value of $N_D(\tau, \tau)$ is not given by the second maximum data point shown in the figure, since the value of this point is obtained from a logarithmic average and is less than $N_D(\tau, \tau)$.

for the conformational equilibration observed in the kinetically selected subensemble.

The results on the mutant H64L contrast with those on native MbCO, where the geminate amplitude of the kinetically selected population was found to be significantly larger than that of the full ensemble, both in 75% glycerol (Tian et al., 1992) and in aqueous solution (Tian et al., 1993). The results of additional measurements on native MbCO at pH 4.9 in 75% glycerol solution at 273 K with delays of 100 ns, 30 μs, 100 μs, and 1 ms (Figure 3) confirm these previous conclusions. For $\tau = 100$ ns, the geminate amplitude of $N^*(t, \tau)$ is significantly larger than that of $N_S(t)$ (Figure 3, upper left panel). This demonstrates that $P_i^*(\tau = 100 \text{ ns}) \neq P_i$ in native Mb, in contrast to the H64L mutant. When the delay time τ increases, the difference between $N^*(t, \tau)$ and $N_S(t)$ decreases, and at $\tau = 1$ ms (lower right panel) $N^*(t, \tau)$ and $N_S(t)$ are identical within experimental error, indicating that conformational averaging is complete. By changing the delay time τ, we can determine the conformational equilibration rate.

The nature of the slowly interconverting conformations in native Mb is suggested by the similarity between the geminate kinetics of the kinetically selected subpopulation and the kinetics of the full ensemble when the pH is lowered (Tian et al., 1992). Reduced pH increases the population of the open conformation (Morikis et al., 1989), in which His64 is displaced from the heme pocket (Quillin et al., 1992). The increased geminate amplitude at lower pH is consistent with the faster geminate recombination observed for the open (A_0) conformation (Ansari et al., 1987). Furthermore, as long as $\lambda\tau \ll 1$, eq 6a predicts that the proportion of the fast rebinding [$N_0(t) < N_1(t)$] open conformation, and thus the geminate amplitude, will be enhanced in the kinetically selected subpopulation relative to the full ensemble ($P_0^* > P_0$).

We thus explore the hypothesis that two kinetically distinct conformations are sufficient to describe the kinetic response of native MbCO at room temperature; that is, that summation over only two conformations $i = 0, 1$ (representing the open and closed conformations) in eqs 4 and 5 will adequately describe both single- and double-pulse experiments at all pH values and time delays. Testing this hypothesis requires appropriate choices for the kinetics, $N_i(t)$, of an ensemble which starts with 100% population of the open or closed states before CO photolysis. We use an empirical function of the form

$$N_i(t) = I^i_{g1} e^{-(k^i_{g1}t)^{\beta i}} + I^i_{g2} e^{-k^i_{g2}t} + I^i_s e^{-\langle k_s \rangle t} \qquad (18)$$

where $I^i_{g1} + I^i_{g2} + I^i_s = 1$ (in aqueous solution $I^i_{g2} = 0$). Since the kinetic selection results in Figure 3 and in previous work (Tian et al., 1993) indicate that conformational interconversion is rapid compared to the bimolecular phase, bimolecular rebinding takes place at a pH-dependent average rate $\langle k_s \rangle$ determined by the equilibrium populations of the open and closed conformations of the deoxy protein, independent of whether the system started in the open or the closed conformation. The kinetic selection results also suggest that conformational interconversion is incomplete during the geminate phase either in 75% glycerol (Figure 3) or in aqueous solution (Tian et al., 1993). Thus we expect the amplitudes and rates, used to describe this phase, to differ depending on whether the system starts in the open or closed state. In general, the overall kinetics are fit to

$$D(t) = D_0 N_S(t) = D_0 \sum_i P_i N_i(t) \qquad (19)$$

where D_0 is a scaling factor that allows comparison of the fit with the measured equilibrium absorbance change at time zero ($D_0 = 1$ if there is perfect agreement between the fit extrapolated to $t = 0$ and the measured equilibrium absorbance change; Tian et al., 1995a) and the functions $N_i(t)$ are given by eq 18.

However, before attempting the fits based on state superposition, we can characterize the geminate kinetic data by first fitting the overall kinetics using a single function (eq 18 with no i dependence) to determine the overall amplitudes and rates. The results of such fits for kinetic data obtained in different solvents as a function of pH are given in Table 1. If we now use the overall geminate amplitude, I_{g1}, to rescale the geminate kinetics as shown in Figure 4, we find a striking difference in behavior for the geminate kinetics as a function of pH when the aqueous and 75% glycerol solutions are compared. In aqueous solution at 273 K, the geminate rate increases by a factor of ~5 when the pH is lowered from 7 to 4.6. In contrast, for the 75% glycerol solution at 264 K, the first geminate phase at each pH (7.0, 5.5, 5.3, and 4.9) is almost perfectly overlapped after rescaling, demonstrating that the rate of the first geminate phase of MbCO rebinding is independent of pH

Table 1: Phenomenological Fitting Results of MbCO Rebinding Kinetics[a]

solution	pH	I_{g1} (%)	k_{g1} ($\times 10^6$ s^{-1})	β	I_{g2} (%)	k_{g2} ($\times 10^5$ s^{-1})	I_s (%)	k_2 ($\times 10^2$ s^{-1})
aqueous	7.0	9.6	1.6	0.5			90	2.8
(273 K)	6.0	10	1.9	0.5			90	3.5
	5.7	12	2.3	0.5			88	4.2
	5.5	12	2.3	0.5			88	4.8
	5.2	14	3.1	0.5			86	6.9
	5.0	14	3.5	0.5			86	8.2
	4.8	17	5.1	0.5			83	11
	4.6	19	6.7	0.5			81	13
	4.4	24	11	0.5			76	17
75% glycerol	7.0	30	3.1	0.5	13	4.5	57	2.9
(264 K)	5.5	43	3.2	0.5	12	5.8	45	3.5
	5.3	49	3.3	0.5	13	5.4	38	3.9
	4.9	58	3.4	0.5	11	6.2	31	4.1

[a] The MbCO rebinding kinetics are fit to eq 18. The *i* superscripts are dropped. All parameters vary freely at each pH except $\beta = 0.5$ and (for aqueous solution data) $I_{g2} = 0$.

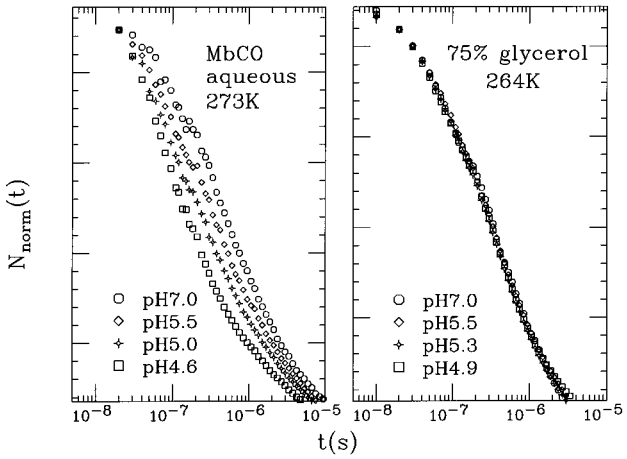

FIGURE 4: Comparison of the geminate kinetics of MbCO as a function of pH in aqueous solution (left panel) and in 75% glycerol solution (first geminate phase, right panel). The kinetics $N_S(t)$ were rescaled for comparison by normalizing the first geminate phases and shifting the data for display on a scale of 0 to 1 [e.g., $N_{norm}(t) = 1 - [1 - N_S(t)]/I_{g1}$ is plotted].

in 75% glycerol solution. As a result, when we use superposition to analyze the rebinding kinetics of MbCO, we constrain $k^0_{g1} = k^1_{g1} = k_{g1}$ and $\beta^0 = \beta^1$ in glycerol solution, while in aqueous solution the second term of eq 18 is dropped ($I^{0,1}_{g2} \rightarrow 0$) and $k^0_{g1} \neq k^1_{g1}$.

In Figure 5 we present the CO rebinding kinetics of MbCO as a function of pH at 273 K in aqueous solution along with the results of the superposition analysis using the spectroscopically observed open (P_0) and closed (P_1) state populations. The solid lines are fits using eqs 18 and 19 (with $I^{0,1}_{g2} = 0$). In order to determine values for the common pH-independent parameters I^{0}_{g1}, k^0_{g1}, I^1_{g1}, and k^1_{g1}, we used a global minimum χ-square fitting analysis to simultaneously fit the data at four pH values (pH 7, 6, 5, and 4.6) with $\beta = 0.5$. P_0 and P_1 were constrained by $P_0 + P_1 = 1$ and

$$\frac{P_0}{P_1} = K_p \frac{1 + 10^{pH - pK_0}}{1 + 10^{pH - pK_1}} \qquad (20)$$

Equation 20 was used with values $pK_0 = 6.0$, $pK_1 = 3.8$, and $K_p = 4.3$, previously shown to describe the equilibrium between open and closed populations as determined from

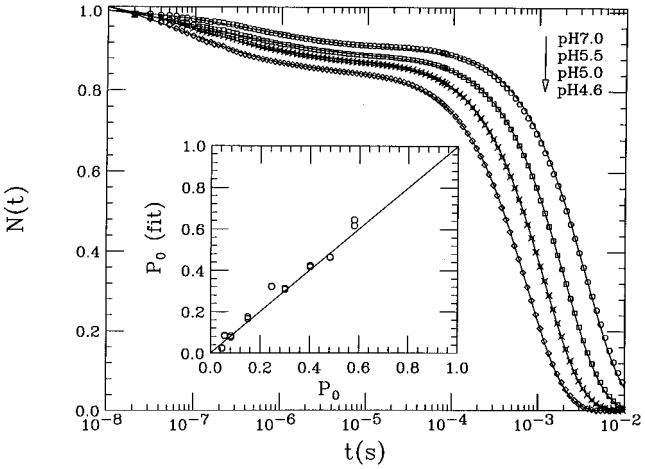

FIGURE 5: Rebinding kinetics of MbCO as a function of pH in aqueous solution at 273 K, analyzed using the open- and closed-state superposition model. The solid lines are the fits using eqs 18 and 19 with $I^{0,1}_{g2} = 0$. The pH-independent parameters $I^{0,1}_{g1}$, $k^{0,1}_{g1}$, and β from Table 2 are fixed in the fit, while the pH-dependent parameters P_0, $\langle k_s \rangle$, and the scaling factor D_0 are allowed to vary. The inset presents the comparison of the calculated P_0 from eq 20 with P_0(fit) from the fit of the kinetics at each pH.

pH-dependent infrared and Raman measurements (Morikis et al., 1989). The pH-independent kinetic parameters determined by this procedure are listed in Table 2. These parameters were then fixed and the data at all pH values (8 data sets for aqueous solution) were fit again using eqs 18 and 19 with the remaining parameters (P_0, $\langle k_s \rangle$, and D_0) free to vary at each pH. The inset of Figure 5 compares the values of P_0(fit) determined from this procedure with the values P_0 calculated from eq 20. The good agreement indicates that the kinetic inhomogeneity of native MbCO can be modeled as a superposition of open and closed states using the populations observed in the IR and Raman measurements. (It should be noted that the analysis of the geminate phase of the aqueous solution in Table 1 fits *N* pH-dependent data sets with 2*N* free parameters, while the superposition of states analysis in Table 2 uses only 4 free parameters.)

For MbCO in 75% glycerol solution at 264 K, we fixed the values of P_0 at pH 7 and 5.5 to the spectroscopic values found in aqueous solution and let the populations at lower pH vary with the other kinetic parameters in a global minimum χ-square simultaneous fit of the data at all four pHs. Then the data were fit again, allowing P_0, $\langle k_s \rangle$, and D_0 to be varied at all pHs, with all other kinetic parameters being fixed. Figure 6 displays the results of the fitting analysis as a function of pH. The detailed results are listed in Table 2. The inset shows that the values of P_0 obtained from the least-squares fit are somewhat larger than the predictions of eq 20, suggesting that glycerol may have a small effect on the open and closed populations.

The kinetic parameters of the open and closed states derived from the above fitting procedure lead to a *prediction* through eqs 6a, 14b, and 18 for the kinetics $N^*(t, \tau)$ of the subpopulation selected in double-pulse experiments. This prediction provides a critical test for the two-state superposition hypothesis. In Figure 7 we compare the double-pulse kinetics predicted by eq 14b in the inhomogeneous limit [$P^*_i(\lambda\tau \ll 1)$ is given by eq 6a] with the results of kinetic selection measurements. The left panel shows results for MbCO in pH 5.0 aqueous solution at 273 K, with a delay

Table 2: Superposition Analysis of MbCO Rebinding Kinetics[a]

		pH-independent parameters[b]				
		I^i_{g1} (%)	k^i_{g1} ($\times 10^6$ s^{-1})	β	I^i_{g2} (%)	k^i_{g2} ($\times 10^4$ s^{-1})
aqueous (273 K)	A_0	32	13	0.50		
	A_1	9.3	1.4	0.50		
35% glycerol[c] (273 K)	A_0	57	5.4	0.50		
	A_1	5.6	5.4	0.50	5.6	29
75% glycerol (293 K)	A_0	85	11	0.45		
	A_1	8.1	11	0.45	3.7	44
75% glycerol (273 K)	A_0	75	5.0	0.63	18	27
	A_1	16	5.0	0.63	11	11
75% glycerol (264 K)	A_0	89	3.1	0.60	11	17
	A_1	26	3.1	0.60	16	5.3

	pH-dependent parameters aqueous, 273 K								
pH	7.0	6.5	6.0	5.5	5.2	5.0	4.8	4.6	4.4
P_0(fit) (%)	2.6	8.3	8.4	18	32	31	42	46	63
D_0[d]	1.01	1.04	1.02	1.02	1.08	1.06	1.09	1.05	0.89
$\langle k_s \rangle$ ($\times 10^2$ s^{-1})	2.8	3.4	3.5	4.8	6.9	8.3	11	13	17

	pH-dependent parameters 75% glycerol							
	264 K				273 K		293 K	
pH	7.0	5.5	5.3	4.9	7.0	4.9	7.0	5.2
P_0(fit) (%)	5.0	20	29	41	5.0	39	5.0	31
D_0	1.05	1.07	1.06	1.01	1.09	1.07	1.03	1.10
$\langle k_s \rangle$ ($\times 10^2$ s^{-1})	3.7	3.4	4.0	4.0	4.2	6.2	6.5	13

[a] The table contains the results of a global fit of eqs 4 and 18 to pH-dependent MbCO kinetics. Parameters in the upper half are constrained to have the same value at all pH values. [b] A_0 represents the "open" state and A_1 represents the "closed" state. [c] The pH-dependent parameters of MbCO in 35% glycerol at 273 K are not shown in the table. The P_0(fit), $\langle k_s \rangle$, and D_0 values are 5.0% and 29%; 4.4×10^2 and 9.5×10^2 s^{-1}, and 1.01 and 1.08 for pH 7.0 and 5.3, respectively. [d] D_0 is a scaling factor that allows comparison of the fit with expected equilibrium absorbance change, ΔA_{eq}, at time zero. $D_0 = 1$ if the fit perfectly agrees with the expected equilibrium absorbance change. $D_0 = 1-1.1$ indicates a good fit because $\Delta A_{eq} < \Delta A_{max}$, due to the effect of the protein relaxation.

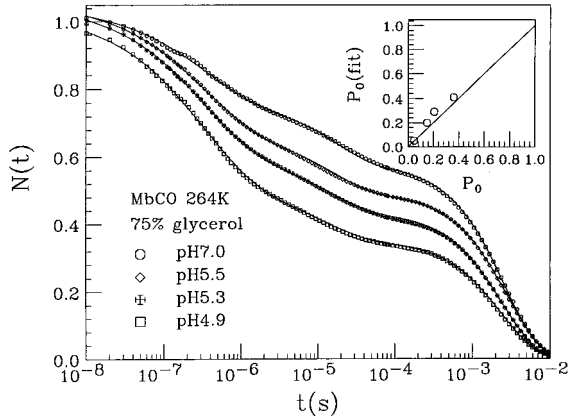

FIGURE 6: Rebinding kinetics of MbCO as a function of pH at 264 K in 75% glycerol solution, analyzed with the open- and closed-state superposition model. The solid lines are fits using eqs 18 and 19. The pH-independent parameters $I^{0,1}_{g1}$, $k^{0,1}_{g1}$, $I^{0,1}_{g2}$, $k^{0,1}_{g2}$, and $\beta^{0,1}$ from Table 2 are fixed in the fit, while the pH-dependent parameters P_0, $\langle k_s \rangle$, and the scaling factor D_0 are allowed to vary. The inset presents the comparison of the calculated P_0 from eq 20 with P_0(fit) determined by the fit at each pH.

time $\tau = 80$ ns, while the right panel shows MbCO in pH 5.3 75% glycerol solution at 264 K, with a delay time $\tau = 1$ μs. The data and prediction were both scaled by a factor of $1/\phi^{(2)}$ for comparison of $N_S(t)$ and $N^*(t)$. The good

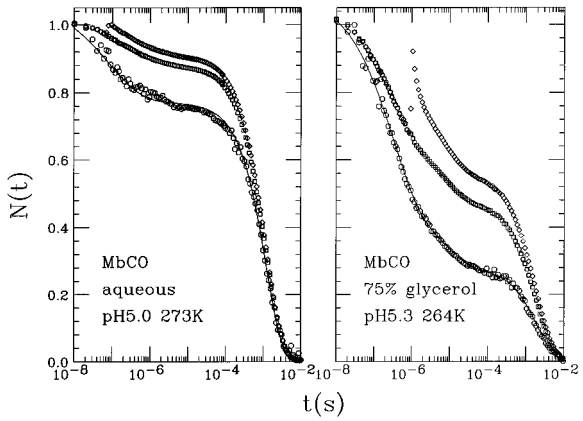

FIGURE 7: Comparison between the $N^*(t, \tau)$ predicted from the superposition analysis using parameters from Table 2 and the $N^*(t, \tau)$ determined from double-pulse experiments on MbCO in pH 5.0 aqueous solution at 273 K with 80-ns delay (left) and in pH 5.3 75% glycerol solution at 264 K with 1-μs delay (right). The circles represent the kinetics of the rephotolyzed ensemble, $CN^*(t, \tau)$. $C = 1/\phi^{(2)}$ is equal to 1.0 for aqueous and 1.2 for 75% glycerol solution. The solid lines are predictions based on the superposition analysis and the parameters in Table 2. Only the scaling factor D_0 is allowed to vary; D_0 is equal to 1.09 for both solutions.

agreement between the experimental results (open circles) and the predictions (solid lines) of eqs 6a, 14b, and 18 with no free parameters (except $D_0 = 1.09$) lends decisive support to the hypothesis that only the open and closed states contribute independently to geminate CO recombination (on time scales $\geq \tau$) under the experimental conditions shown in Figures 5−7.

In addition to providing a critical test of the two-state superposition model, the above analysis provides the background needed for a quantitative determination of the interconversion rate between the open and closed states (Tian et al., 1992, 1993). As $\lambda\tau$ increases, the populations $P_i^*(\tau)$ in the kinetically selected subpopulation are affected by protein conformational interconversion as well as by recombination so that the limit in eq 6a no longer applies. By monitoring the change in the value $P_0^*(\tau)$ needed to describe double-pulse measurements at variable τ between the two limits given by eq 6a,b, we can determine the rate λ of equilibration between the open and closed states, as shown in Figure 8. The left panel shows that the geminate yield of the rephotolyzed fraction decreases at longer delay times, as the population $P_0^*(\tau)$ of the fast-rebinding A_0 state approaches the equilibrium value P_0. The solid lines through the data are fits using eqs 6a, 14b, and 18 with fixed values for the pH-independent parameters (Table 2) but with $P_0^*(\tau)$, $\langle k_s \rangle$, and D_0 free to vary. The pH-independent parameters were obtained from the previously described simultaneous fit of the pH-dependent data. In the right panel of Figure 8 we plot the quantity

$$\Phi(\tau) = \frac{P_0^*(\tau) - P_0}{P_0^*(\lambda\tau \ll 1) - P_0} \qquad (21)$$

as a measure of the relaxation of the kinetically selected population $P_0^*(\tau)$ to the equilibrium value P_0, normalized by $P_0^*(\lambda\tau \ll 1) - P_0$, which is calculated from eq 6a for each delay. The quantity $P_0^*(\tau)$ contains the information relevant to substate interconversion. The solid lines in the

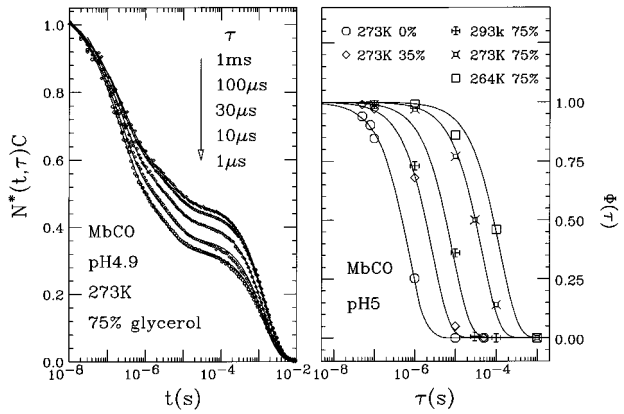

FIGURE 8: Interconversion rate between the "open" and "closed" states of MbCO determined by the double-pulse experiments. The left panel shows the kinetics of the rephotolyzed population $N^*(t, \tau)$ of MbCO in pH 4.9 75% glycerol solution at 273 K with different delay times. $N^*(t, \tau)$ was normalized using the amount of rephotolysis ($C = 1.3$, 1.3, 1.5, 1.3, and 1.4 for $\tau = 1$, 10, 30, 100, and 1000 μs, respectively). The solid lines are the superposition fit using parameters from Table 2, while the parameters P_0, $\langle k_s \rangle$, and D_0 are allowed to vary. The right panel shows the quantity $\Phi(\tau) = [P_0^*(\tau) - P_0]/[P_0^*(\lambda\tau \ll 1) - P_0]$ (eq 21) versus the delay time, τ. $P_0^*(\tau)$ is determined by the fit with eqs 14b and 18 and reflects the effects of both rebinding kinetics and conformational interconversion. $P_0^*(\lambda\tau \ll 1)$ is calculated from eq 6a and is determined only by conformational differences in rebinding kinetics. P_0 is from eq 20. The solid lines are exponential fits, $\Phi(\tau) = e^{-\lambda\tau}$, to the relaxation in different solvents at different temperatures. The values of λ are listed in Table 3.

Table 3: Interconversion Rates of the Open and Closed States of MbCO at pH 5[a]

solution	T (K)	λ (s^{-1})
aqueous	273	1.4×10^6
35% glycerol	273	3.7×10^5
75% glycerol	293	1.2×10^5
75% glycerol	273	2.3×10^4
75% glycerol	264	8.1×10^3

[a] λ is the sum of the forward and reverse interconversion rates for the transition between the open and closed states of MbCO, obtained from the fit $\Phi(\tau) = \exp(-\lambda\tau)$.

right panel are fits of the $P_0^*(\tau)$ relaxation to equilibrium assuming an exponential decay, $\Phi(\tau) = \exp(-\lambda\tau)$. The values obtained for the interconversion rates, λ, are listed in Table 3. The interconversion times between the open and closed states in 75% glycerol solution are 1.2×10^5, 2.3×10^4, and 8.1×10^3 s^{-1} at 293, 273, and 264 K, which agree very well with extrapolation of infrared measurements of the $A_0 \rightarrow (A_1, A_3)$ transition rates observed at somewhat lower temperatures (Young et al., 1991). In aqueous solution at 273 K, we obtain a significantly faster interconversion rate of 1.4×10^6 s^{-1}, which is the first such measurement in aqueous solution.

The adequacy of the simple two-state superposition model in describing the results above does not exclude possible contributions from more rapidly interconverting conformations at lower temperature or shorter times. We studied the CO rebinding kinetics of H64L MbCO as a function of temperature using double-pulse methods and found that above ~270 K the system is effectively "homogeneous" on the ~100-ns time scale. In the left panel of Figure 9, we present a two-pulse kinetic selection measurement on the mutant H64L MbCO in 75% glycerol at 264 K with a delay time of 80 ns. $N^*(t, \tau)$ appears to deviate from $N_s(t)$ (between

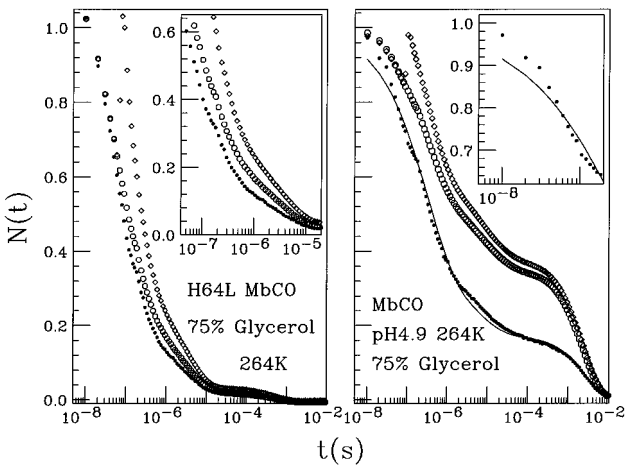

FIGURE 9: (Left panel) Double-pulse experiments on H64L MbCO in 75% glycerol solution at 264 K with 80-ns delay. The solid dots are the rephotolyzed ensemble kinetics, $CN^*(t, \tau)$. The inset is an expansion figure. (Right panel) Comparison between the superposition prediction and double-pulse experimental results of MbCO in pH 4.9 75% glycerol solution at 264 K with 100-ns delay. The solid dots are the kinetics of the rephotolyzed population, $CN^*(t, \tau)$. The solid line is the superposition analysis prediction from eqs 6a, 14b, and 18 using the parameters from Table 2 and leaving D_0 free to vary ($D_0 = 1.0$). The inset is an expansion figure.

10^{-7} and 10^{-6} s), suggesting that interconversion among substates of tier 1 is incomplete on the 80-ns time scale at 264 K. Similar results are apparent with $\tau \simeq 100$ ns in native MbCO at 264 K (75% glycerol), since the double-pulse kinetic data begin to deviate from the prediction of the two-state model using the parameters in Table 2 (see the right panel of Figure 9), in contrast to the successful prediction at longer delay times (Figure 7). This is consistent with the idea that the open and closed states represent only the upper level of a conformational hierarchy (Frauenfelder et al., 1991). We suggest that the characterization of such a hierarchy is best organized according to interconversion time scales. Evidently, the (tier 1) protein fluctuations that govern the heme iron equilibrium position (Šrajer et al., 1988) extend somewhat beyond the 100-ns time scale at 264 K in 75% glycerol. However, above 264 K, or for delay times $\tau \geq 1$ μs at 264 K, the two-state model successfully describes the double-pulse measurements of MbCO in both aqueous and 75% glycerol solution.

Since the substates of MbO_2 have not been independently probed by IR methods, kinetic selection experiments provide a unique test for contributions for slowly interconverting, kinetically distinct MbO_2 substates at room temperature. MbO_2 is not completely photolyzed by the first pulse when probed on the 10-ns time scale, and thus, the conformation dependence of $\phi_i^{(1,2)}$ is not well determined by measuring $N_S(t)$. As a result, we have to treat $\phi_i^{(1,2)}$ of MbO_2 as if it were conformation-dependent. As discussed in the Theory section, when the ensemble is incompletely photolyzed and $\phi_i^{(1,2)}$ is conformation-dependent, the two photolyzing pulses must have equal intensity in order to use eq 3 to test for conformational equilibration [e.g., by blocking the first pulse to measure $N_{S2}(t)$ as discussed following eq 16]. Figure 10 presents a double-pulse experiment on MbO_2 in 75% glycerol solution at 273 K with a 70-ns delay (open diamonds). In the left panel, we directly compare $N^*(t, \tau)$ (solid dots) with the single-pulse kinetics $N_{S2}(t)$ (plus signs)

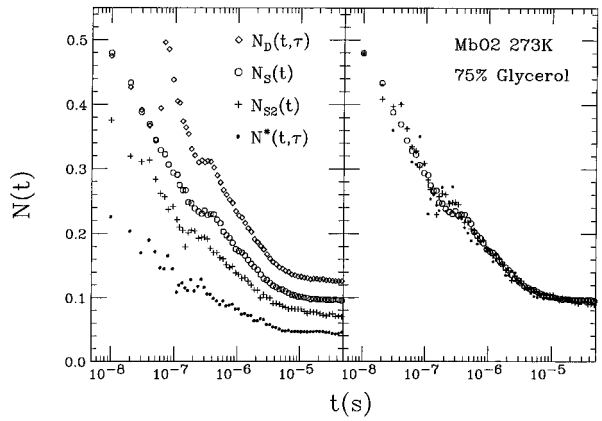

FIGURE 10: Double-pulse experiments on MbO_2 in 75% glycerol at 273 K with 70-ns delay. In the left panel, the open circles are the single-pulse kinetics, $N_S(t)$. The open diamonds are the double-pulse kinetics, $N_D(t, \tau)$. The filled circles are the kinetics of the rephotolyzed population, $N^*(t, \tau)$. The plus signs are the single-pulse kinetics, $N_{S2}(t)$, when the sample is photolyzed only by the second pulse (see Figure 2). The right panel is a comparison of $N_S(t)$ with the rescaled $N^*(t, \tau)$ and $N_{S2}(t)$.

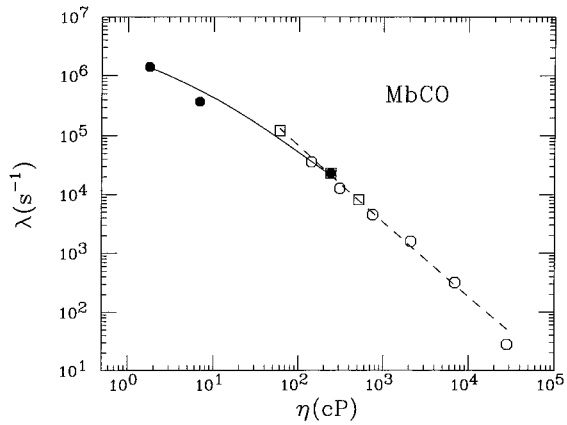

FIGURE 11: Viscosity-dependent open/closed interconversion rates for MbCO. The open circles are data from transient IR measurements of Young et al. (1991) in 75% glycerol solution at 280−230 K. The open squares are the data from kinetic selection experiments in 75% glycerol solution at 293, 273, and 264 K. The solid circles are the data from kinetic selection measurements at 273 K in aqueous, 35% glycerol, and 75% glycerol solution. The whole data set was fit with eq 22. The solid line represents the viscosity dependence at 273 K (solid circles) and the dashed line is the temperature dependence for a fixed 75% glycerol solvent composition.

that result from photolysis by only the second pulse *without scaling* (this automatically satisfies the equal photolysis conditions; see Figure 1, right panel). The significant difference between $N^*(t, \tau)$ (∼25% missing amplitude) and $N_{S2}(t)$ (∼40% missing amplitude) suggests that MbO_2 is inhomogeneous on the 70-ns time scale at 273 K. In order to extract more information from the MbO_2 kinetics, $N_S(t)$, $N^*(t, \tau)$, and $N_{S2}(t)$ were normalized and compared (right panel of Figure 10). The result shows that, after renormalization, these curves are overlapped within the errors. One simple explanation is that MbO_2 has two conformations with very different photolysis yields and the kinetics after 10-ns arises from only one conformation ($\phi_1^{(2)} = 1$, $P_1 = 0.64$), while the other component is not photolyzed ($\phi_2^{(2)} = 0$, $P_2 = 0.36$) by a 10-ns pulse. This explanation is consistent with the quantum yield study of MbO_2 at 8 K, which found that only a fraction (0.4 ± 0.1) of the sample could be photolyzed by a 40-ps pulse (Chance et al., 1990).

DISCUSSION

(A) Transitions among the "A-States". Transition rates among the "A-states" of MbCO in 75% glycerol solution have been measured previously using infrared spectroscopy in combination with flash photolysis (230−280 K) and pressure release (190−220 K) techniques (Young et al., 1991; Frauenfelder et al., 1990; Iben et al., 1989). The double-pulse kinetic selection experiments presented here also monitor interconversion rates between the A_0 (open) and $A_1 + A_3$ (closed) states of myoglobin. In Figure 11, we present a comparison of the MbCO open and closed interconversion rates (λ) as a function of viscosity (η) using all available data at pH ∼ 5−6. The rates from double-pulse experiments in 75% glycerol solution at 264, 273, and 293 K (open squares) agree very well with the rates obtained from IR flash photolysis experiments in 75% glycerol solution at 230−280 K (Young et al., 1991; open circles). The solid circles are the data from double-pulse experiments at 273 K in aqueous, 35% glycerol, and 75% glycerol solutions (Table 3). The solid points at low viscosity ($\lambda \sim 10^6$ s^{-1}) represent the first measurements of the conformational interconversion rates for transitions between the open and closed states of Mb as physiological conditions are approached (aqueous, 273 K).

In analogy with the treatment of solvent viscosity effects on protein conformational relaxation by Ansari et al. (1992), we express the temperature- and viscosity-dependent interconversion rates as

$$\lambda = \lambda_+ + \lambda_- = \frac{K}{\sigma + \eta}(e^{-(E_0-\Delta)/k_BT} + e^{-E_0/k_BT}) \quad (22)$$

where $\lambda_{+,-}$ are the transition rates between the open and closed conformations, k_B is the Boltzmann constant, T is temperature, and η is viscosity.[7] The parameter K is independent of viscosity and temperature, while σ represents the contribution of the protein to the total friction and E_0 is the energy barrier for the transition from the open to the closed state.

We simultaneously fit the temperature-independent data [$\lambda(\eta, 273\ \text{K})$, solid circles, solid line] and the temperature-dependent data [$\lambda(\eta, T)$, open symbols, dashed line] using eq 22, with the free energy difference between the open and closed states fixed to the value $\Delta = -k_BT \ln (P_0/P_1) \simeq 1.7$ kJ/mol determined from eq 20 at pH 5. The unknown parameters are found to be $K = 1.9 \times 10^9$ cP/s, $\sigma = 2.2$ cP, and $E_0 = 16 \pm 5$ kJ/mol.[8] As for the "tier 1" relaxation process studied by Ansari et al. (1992), the value obtained for σ indicates that when $\eta \leq 1$ cP (aqueous solution), the contribution of the viscosity to λ is small, so that protein

[7] The viscosity of water is taken from the *Handbook of Chemistry and Physics* (1984, 65th edition). The viscosity of the sample in 75% glycerol as a function of temperature was calculated from the empirical equation of Hasinoff et al. (1977), based on the measurement with high percentages of glycerol [>50% (wt)]: $\log \eta = aG^3 + bG^2 + cG + dG/T + eG^2/T^2 + f/T + g/T^2 + h$, where G is the (w/w) percentage of glycerol, T is temperature (in kelvins), $a = 5.43 \times 10^{-6}$, $b = -1.31 \times 10^{-3}$, $c = 1.24 \times 10^{-1}$, $d = -2.28 \times 10^{1}$, $e = 5.86 \times 10^{1}$, $f = -4.15 \times 10^{2}$, $g = 2.88 \times 10^{5}$, and $h = -5.56$. The viscosity of 35% glycerol solution is also calculated from this equation as an approximation. Note that E_0 cannot be compared directly to the phenomenological "energy barrier" $E_B = 10$ kJ/mol that Young et al. obtained by fitting λ with a non-Arrhenius equation $\lambda(T) = A_B \exp[-(E_B/k_BT)^2]$.

friction and temperature dominate the interconversion rate λ. However, when $\eta \gg \sigma$, the solvent friction (viscosity) controls λ.

External conditions significantly affect the interconversion between the open and closed states. Figures 8 and 11 show that the interconversion rate decreases when the temperature is lowered or the concentration of glycerol in the solution increases, both of which increase the viscosity. For a sample in 75% glycerol solution and a temperature change from 260 to 290 K, the exponential term in eq 22 changes only by about a factor of 2 while the viscosity-dependent term changes by about an order of magnitude. Under these conditions, we see that the viscosity has a much larger influence on the interconversion rate than does the temperature.[9]

The conformational space of proteins has been classified using a tier concept with different time scales for interconversion among states of a given tier (Young et al., 1991). In 75% glycerol at 264 K, the interconversion rate between the open and closed states of Mb was found to be 8.1×10^3 s^{-1} (Table 3). On the other hand, on the basis of the results of Figure 7 and 9, we can estimate the fluctuation rate among the substates within the open conformation to be in the range 10^6-10^7 s^{-1}, more than 2 orders of magnitude faster than the interconversion between the open and closed states. This estimate can be compared with relaxation rates extrapolated from previous low-temperature pressure-release experiments (Iben et al., 1989), which were carried out between 165 and 185 K on MbCO (it should be noted that the structural changes associated with "tier 1" in this study probably involve localized distal pocket configurations rather than proximal histidine−heme geometry changes). In these experiments, the "tier 1" relaxation rate, k_r, was fit using $k_r(T) = k_0 \exp[-(T_0/T)^2]$ with parameters $\log (k_0/\text{s}^{-1}) = 17 \pm 2.5$, $T_0 = 1130 \pm 80$ K, so that $k_r(264\text{ K}) \sim 10^{9\pm3.5}$ s^{-1}. In contrast, extrapolation of the pressure-release analysis of Young et al. (1991) for "tier 1" relaxation leads to $\log (k_0/\text{s}^{-1}) = 7$ and $T_0 = 842$ K, so that $k_r(264\text{ K}) = 4.7 \times 10^2$ s^{-1}, which suggests that the localized distal pocket relaxation rates are not yet well-defined at room temperature.

(B) Nonexponential Geminate Kinetics. Although nonexponential geminate kinetics are observed at both low temperature and room temperature, the sources of the nonexponential behavior are totally different. Due to the large geminate amplitude at low temperature, the nonexponential kinetics directly reflect a distribution of geminate rebinding rates. However, at room temperature, the small geminate amplitude observed for native MbCO at pH 7 suggests that ligand escape rather than rebinding is the major contribution to the geminate rate (Tian et al., 1992). In contrast, the kinetics of the mutant H64L have a large geminate amplitude and the double-pulse experiments (Figure 2) show that the interconversion among the different (tier 1) conformations is fast enough to average the ensemble even though it displays nonexponential geminate rebinding. This result supports the conclusion outlined in an earlier report

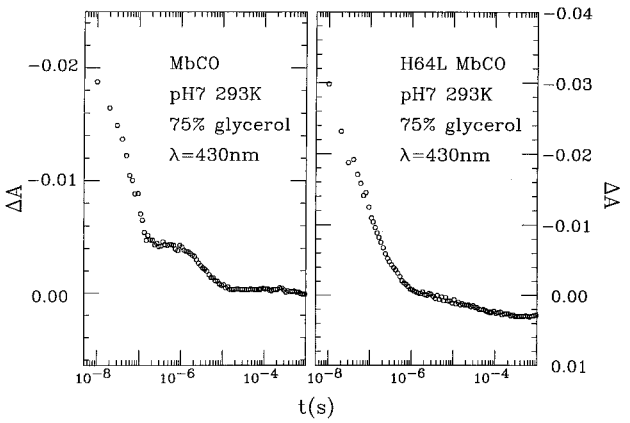

FIGURE 12: Transient absorbance measurements of mutant H64L and native MbCO in pH 7 75% glycerol solution at 293 K. The probe wavelengths are both at the isosbestic point between MbCO and deoxyMb near 430 nm (see footnote 10).

(Tian et al., 1992), where we argued that distributed rebinding rates could not account for the nonexponential character of the MbCO geminate kinetics at room temperature, contrary to a previous suggestion (Steinbach et al., 1991).

In the same report, we also suggested that the small spectral shifts of the Mb Soret band observed during the geminate phase (Tian et al., 1992; Lambright et al., 1991; Ansari et al., 1992) were related to structural changes taking place in the heme pocket that impart a fundamental time dependence to the geminate rate. It is conceivable that the interconversion between the open and closed states may contribute to the observed spectral shifts, since the Soret absorption bands of these conformations differ slightly (Morikis et al., 1991). The mutant H64L, which lacks tier 0 (Balasubramanian et al., 1993), offers a basis for comparison (Figure 12).[10] We note the appearance of a distinct additional ~5-μs relaxation following CO photolysis from the native protein (Figure 12, left panel) under the same experimental conditions (75% glycerol, 293 K). We suggest that this additional spectral shift is the signature of the open and closed conformational equilibration at $\lambda^{-1} \sim 8$ μs (Table 3).

However, measurements at the MbCO/deoxyMb equilibrium isosbestic point (~430 nm) of the mutant H64L at 293 K (Figure 12, right panel) still exhibit evidence of a time-dependent spectral shift, consistent with evolution of the heme pocket structure on a time scale (10−100 ns) that is somewhat more rapid than the open/closed interconversion in the native protein. A review of the available spectroscopic evidence on protein relaxation suggests (Sage et al., 1995) that evolution of the Soret band on the nanosecond time scale (Lambright et al., 1991; Tian et al., 1992; Ansari et al., 1994) probes the long-time tail of the picosecond relaxation process studied in some detail at room temperature using band III (Jackson et al., 1994). In principle, this process may include both proximal and distal components. Along with the evidence for tier 1 equilibration before 100 ns presented here, this is consistent with similar time scales for protein relaxation and conformational equilibration (Post et al., 1993).

[9] The close agreement (see Figure 11) between the present data at pH 5 and that of Young et al. (1991) at pH 5.7 indicates that the open/closed interconversion rate is not strongly pH-dependent. Note that protonation of the distal histidine is too slow to contribute to the observed equilibration process at pH 5, based on the proton association rate 1.5×10^{10} M^{-1} s^{-1} reported for imidazole in aqueous solution at 298 K (Eigen et al., 1960).

[10] The isosbestic point is operationally defined as the wavelength for which $\Delta A = 0$ at the end of the geminate phase (~20 μs for native MbCO and ~2 μs for H64L).

In summary, for $T > 264$ K the tier 1 fluctuation rate is faster than the CO geminate kinetics, so that the kinetic response is independent of initial (tier 1) conformation, but the long-time tail of the protein relaxation may contribute to the nonexponential geminate rebinding. Below 264 K, both protein relaxation and conformational rate distributions may contribute to the nonexponential geminate kinetics. At still lower temperatures (below 180 K), both fluctuation and relaxation processes are "quenched", so that the distribution of rates in the ensemble determines the nonexponential behavior (Steinbach et al., 1991). Rebinding of some ligands, such as NO, is rapid enough that individual protein conformations may contribute independently to the kinetics even at room temperature and be partly responsible for the observed nonexponential kinetics (Gibson et al., 1992).

(C) Analysis of pH-Dependent Kinetics. A simple model involving only two (open and closed) distal pocket conformational states has been developed and used to analyze the pH dependence of the MbCO rebinding kinetics. The bimolecular rebinding and its pH dependence were discussed previously in some detail (Tian, et al., 1992), so the geminate kinetics have been emphasized here. The excellent fit of the pH-dependent geminate rebinding kinetics and the successful prediction of the kinetic response observed in the double-pulse experiments ($\lambda\tau \ll 1$) strongly support this two-state analysis.

The population of the open distal conformation is coupled to distal histidine protonation, and its motion toward the solvent helps to open a pathway for ligand migration. In aqueous solution, the open-state geminate amplitude (I^0_{g1}) is about a factor of 3 larger than the closed-state amplitude (I^1_{g1}), while the open-state geminate rate (k^0_{g1}) is about a factor of 10 larger than the closed-state rate (k^1_{g1}). The significant increases of the amplitude and rate for the open state indicate that it plays an important role in the control of ligand binding at the heme [i.e., $k^0_{BA}/k^1_{BA} \cong (I^0_{g1}k^0_{g1})/(I^1_{g1}k^1_{g1}) \sim 30$]. As a result, the increase of the open state population P_0 at lower pH in aqueous solution significantly affects the geminate as well as the bimolecular kinetics.

In 75% glycerol solution at 264−293 K, $I^0_{g1} \simeq 3I^1_{g1}$, while k^0_{g1} and k^1_{g1} are the same as shown in Figure 4. The equivalence of k^0_{g1} and k^1_{g1} is not completely understood, but it clearly signals major functional differences for the MbCO rebinding reaction when the solvent is altered from aqueous to 75% glycerol solution and indicates that the solvent strongly perturbs the protein−ligand dynamics near room temperature. The significant difference between the pH-dependent kinetics of MbCO in aqueous and 75% glycerol solutions is also supported by observations of the bimolecular rates (see Table 2 at 273 K). When the pH changes from 7 to 4.9, $\langle k_s \rangle$ increases by a factor of ~3.5 in aqueous solution, while it only increases 50% in 75% glycerol solution. This significant difference cannot be explained by the small difference of the open-state population in the two solutions. This suggests that the association rate of the open state (k^0_{on}) must be much larger than for the closed state (k^1_{on}) in aqueous solution[11] but only slightly larger in 75% glycerol solution.

[11] In previous work (Tian et al., 1993), we discussed the association rates of the open and closed states and found that $k^0_{on}/k^1_{on} \sim 20$ in aqueous solution at 273 K; $k_{on} = k_s/[CO]$, and [CO] = 1.57 mM at 1 atm and 273 K.

In another previous study (Sage et al., 1995), we found a downshift of the iron−histidine mode of deoxyMb in 75% glycerol relative to that observed in aqueous solution, indicating a glycerol-induced alteration of the heme pocket structure that might affect the protein dynamics and kinetics. It is also conceivable that glycerol restricts the displacement of the distal histidine, so that the distal pocket does not open as completely as in aqueous solution, resulting in a decrease of k^0_{on}/k^1_{on}.

Finally, we note the pH independence of the geminate rates in 75% glycerol solution (Figure 4) and the similarity of λ and k^1_{g1} in aqueous solution (Tables 2 and 3). While it is possible that these observations are simply coincidental, they do not arise naturally within the superposition model presented here. We have therefore explored a somewhat more complex model, which allows the explicit introduction of the interconversion rates into the observed kinetic response. Such a model has many attractive features, including two geminate phases, each with degenerate eigenvalues that could explain the equivalence of k^0_{g1} and k^1_{g1} in 75% glycerol. In addition, this model can provide a direct link between k^1_{g1} and λ for the aqueous case. Unfortunately, the model suffers from its inability to quantitatively account for the pH dependence of the double-pulse experiments, so we have relied on the more straightforward superposition model in the present analysis.

(D) Limitations of the Experiment and the Two-State Model. The criterion for conformational equilibration embodied in eq 3 is quite general. However, as a practical method, the double-pulse kinetic selection method works best for delay times occurring on time scales during which ~10−80% of the population has rebound after the first pulse. At very short delay times, only a small fraction of the molecules rebind and the signal-to-noise level of $N^*(t, \tau)$ is reduced. A similar limitation occurs at very long delay times (Post et al., 1993; Agmon et al., 1994) when almost all the population has rebound so that $P^*_i(\tau) \simeq P_i$ even before the onset of interconversion.

The two-state model presented here to explain the pH-dependent kinetic data includes the two geminate phases as a population-weighted superposition, while bimolecular rebinding takes place with a single average rate. Under more general circumstances (e.g., at low temperatures when tier 1 interconversion becomes comparable to the geminate rate), a more complex multiple-state model may be needed. However, multiple-state models involve many transition rates, which are difficult to determine uniquely. For example, Ansari et al. (1994) proposed an eight-state model to describe the viscosity-dependent nonexponential geminate rebinding with fast and slow rebinding conformations (Ansari et al., 1994). Since such a large number of parameters (37) are needed in this model, many of them cannot be well determined and some appear to be unphysical (e.g., their relaxed binding barrier $E_{BA} \sim 80$ kJ/mol seems much too large). We have also explored a variety of microscopic models to account for the above data. These will be fully discussed and evaluated elsewhere.

CONCLUSION

The kinetic selection experiments described here provide a powerful tool for measuring the rate of interconversion

among conformational substates of a protein. The interconversion rates between the open and closed states (tier 0) of MbCO are found to lie in the range 10^4-10^6 s^{-1}, depending on solvent and temperature (264−293 K), while the equilibration rate of substates (tier 1) associated with the open and closed states of MbCO in 75% glycerol solution at 264−273 K is found to be faster than 10^6-10^7 s^{-1}. Interconversion between the open and closed states is quite sensitive to environmental conditions, slowing down when the temperature decreases and/or viscosity increases. At very low viscosity (aqueous), temperature plays a major role in controlling the interconversion rate. In contrast, at high viscosity, the temperature is less important and viscosity controls the interconversion rate.

A simple two-state model based on a population-weighted superposition is used to analyze the geminate and bimolecular kinetics. This simple two-state model for myoglobin is strongly supported by the fits to the pH-dependent data and the successful prediction of the kinetic response in double-pulse experiments. In aqueous solution, the geminate rate and amplitude of the open state are significantly larger than those of the closed state, indicating that the open-state conformation plays an important role in the ligand binding from the heme pocket as well as in the overall ligand association and dissociation processes (Tian et al., 1993). In aqueous solution, $\lambda \sim k_{g1}^1$ is consistent with the opening of a pathway for ligand escape upon transition from the closed to the open state.

In 75% glycerol, however, conversion to the open state does not occur until the end of the geminate phase ($\lambda \ll k_{g1}^{0,1}$, $k_{g2}^{0,1}$) so that the ligand must find alternate escape channels. Moreover, the primary geminate rates associated with the open and closed states are found to be equivalent. This observation is not fully understood, but it is consistent with the concept of alternative escape channels and clearly signals major functional differences for the MbCO binding reaction when the solvent is altered, demonstrating a strong perturbation of glycerol on the protein−ligand dynamics near room temperature.

Finally, we have studied the large-amplitude nonexponential geminate rebinding of a Mb mutant, H64L, which lacks the distal histidine and the open and closed (tier 0) substates. Conformational averaging is observed to be complete within 100 ns at room temperature, refuting the suggestion (Steinbach et al., 1991; Chu et al., 1995) that nonexponential geminate kinetics at room temperature are due to a quasistatic distribution of barrier heights, which becomes the source of nonexponential behavior at lower temperature. Studies of the transient absorbance at the equilibrium isosbestic point of the deoxyMb and MbCO (H64L and native) absorption spectra are consistent with time evolution of the protein structure that contributes to the nonexponential behavior.

REFERENCES

Agmon, N., Doster, W., & Post, F. (1994) *Biophys. J. 66*, 1612−1622.

Alben, J. O., Beece, D., Bowne, S. F., Doster, W., Eisenstein, L., Frauenfelder, H., Good, D., McDonald, J. D., Marden, M. C., Moh, P. R., Reinsich, L., Reynolds, A. H., Shyamsunder, E., & Yue, K. T. (1982) *Proc. Natl. Acad. Sci. U.S.A. 79*, 3744−3748.

Ansari, A., Berendzen, J., Braunstein, D., Cowen, B. R., Frauenfelder, H., Hong, M. K., Iben, I. E. T., Johnson, J. B., Ormos, P., Sauke, T. B., Scholl, R., Schulte, A., Steinbach, P. J., Vittitow, J., & Young, R. D. (1987) *Biophys. Chem. 26*, 337−355.

Ansari, A., Jones, C. M., Henry, E. R., Hofrichter, J., & Eaton, W. A. (1992) *Science 256*, 1796−1798.

Ansari, A., Jones, C. M., Henry, E. R., Hofrichter, J., & Eaton, W. A. (1993) *Biophys. J. 64*, 852−868.

Ansari, A., Jones, C. M., Henry, E. R., Hofrichter, J., & Eaton, W. A. (1994) *Biochemistry 33*, 5128−5145.

Antonini, E., & Brunori, M. (1971) *Hemoglobin and Myoglobin in their Reactions with Ligands*, North-Holland, Amsterdam.

Austin, R. H., Beeson, K. W., Eisenstein, L., Frauenfelder, H., & Gunsalus, I. C. (1975) *Biochemistry 14*, 5355−5373.

Balasubramanian, S., Lambright, D. G., & Boxer, S. G. (1993) *Proc. Natl. Acad. Sci. U.S.A. 90*, 4718−4722.

Case, D. A., & Karplus, M. (1979) *J. Mol. Biol. 132*, 343−368.

Caughey, W. S., Shimada, H., Choc, M. G., & Tucker, M. P. (1981) *Proc. Natl. Acad. Sci. U.S.A. 78*, 2903−2907.

Champion, P. M. (1987) in *Proceedings of the International Symposium on Frontiers in Science*, American Institute of Physics Conference Proceedings No. 180 (Chan, S. S., & Debrunner, P. G., Eds.) p 310, American Institute of Physics, New York.

Champion, P. M. (1992) *J. Raman Spectrosc. 23*, 557−567.

Chance, B., Ravilly, A., & Rumen, N. (1966) *J. Mol. Biol. 17*, 525−534.

Chance, M. R., Courtney, S. H., Chavez, M. D., Ondrias, M. R., & Friedman, J. M. (1990) *Biochemistry 29*, 5537−5545.

Chu, K., Ernst, R. M., Frauenfelder, H., Mourant, J. R., Nienhaus, G. U., & Philipp, R. (1995) *Phys. Rev. Lett. 74*, 2607−2610.

Doster, W., Beece, D., Bowne, S., DiIorio, E., Eisenstein, L., Frauenfelder, H., Reinisch, L., Shyamsunder, E., Winterhalter, K., & Yue, K. (1982) *Biochemistry 21*, 4831−4839.

Eigen, M., Hammes, G., & Kustin, K. (1960) *J. Am. Chem. Soc. 82*, 3482−3492.

Frauenfelder, H. (1983) in *Structure and Dynamics: Nucleic Acids and Proteins* (Clementi, E., & Sarma, R. H., Eds.) p 369, Adenine Press, Guilderland, NY.

Frauenfelder, H., Alberding, N. A., Ansari, A., Braunstein, D., Cowen, B. R., Hong, M. K., Iben, I. E. T., Johnson, J. B., Luck, S., Marden, M. C., Mourant, J. R., Ormos, P., Reinisch, L., Scholl, R., Schulte, A., Shyamsunder, E., Sorensen, L. B., Steinbach, P. J., Xie, A. H., Young, R. D., & Yue, K. T. (1990) *J. Phys. Chem. 94*, 1024−1037.

Frauenfelder, H., Sligar, S. G., & Wolynes, P. G. (1991) *Science 254*, 1598−1603.

Gibson, Q. H. (1956) *J. Physiol. 134*, 112−122.

Gibson, Q. H., Olson, J. S., McKinnie, R. E., & Rohlfs, R. J. (1986) *J. Biol. Chem. 261*, 10228−10239.

Gibson, Q. H., Regan, R., Elber, R., Olson, J. S., & Carver, T. E. (1992) *J. Biol. Chem. 267*, 22022−22034.

Hasinoff, B. B. (1977) *Arch. Biochem. Biophys. 183*, 176−188.

Henry, E. R., Sommer, J. H., Hofrichter, J., & Eaton, W. A. (1983) *J. Mol. Biol. 166*, 443−451.

Iben, I. E. T., Braunstein, D., Doster, W., Frauenfelder, H., Hong, M. K., Johnson, J. B., Luck, S., Ormos, P., Schulte, A., Steinbach, P. J., Xie, A. H., & Young, R. D. (1989) *Phys. Rev. Lett. 62*, 1916−1919.

Jackson, T. A., Lim, M., & Anfinrud, P. A. (1994) *Chem. Phys. 180*, 131−140.

Johnson, K. A., Olson, J. S., & Phillips, G. N. (1989) *J. Mol. Biol. 207*, 459−463.

Kerr, E., & Yu, N. T. (1988) in *Biological Applications of Raman Spectroscopy* (Spiro, T. G., Ed.) Vol. 3, pp 39−95, Wiley, New York.

Lambright, D. G., Balasubramanian, S., & Boxer, S. G. (1991) *Chem. Phys. 158*, 249−260.

Morikis, D., Champion, P. M., Springer, B. A., & Sligar, S. G. (1989) *Biochemistry 28*, 4791−4800.

Morikis, D., Li, P., Bangcharoenpaurpong, O., Sage, J. T., & Champion, P. M. (1991) *J. Phys. Chem. 95*, 3391−3398.

Nienhaus, G. U., Mourant, J. R., Chu, K., & Frauenfelder, H. (1994) *Biochemistry 33*, 13413−13430.

Olson, J. S., Mathews, A. J., Rohlfs, R. J., Springer, B. A., Egeberg, K. D., Sligar, S. G., Tame, J., Renaud, J., & Nagai, K. (1988) *Nature (London) 336*, 265−266.

Perutz, M. F., & Mathews, F. S. (1966) *J. Mol. Biol. 21*, 199−202.

Post, F., Doster, W., Karvounis, G., & Settles, M. (1993) *Biophys. J. 64*, 1833−1842.

Quillin, M. L., Brantley, R. E., Johnson, K. A., Olson, J. S., & Phillips, G. N. (1992) *Biophys. J. 61*, A466.

Ringe, D., Petsko, G. A., Kerr, D. E., & Ortiz de Montellano, P. R. (1984) *Biochemistry 23*, 2−4.

Sage, J. T., Morikis, D., & Champion, P. M. (1991a) *Biochemistry 30*, 1227−1237.

Sage, J. T., Li, P., & Champion, P. M. (1991b) *Biochemistry 30*, 1237−1247.

Sage, J. T., Schomacker, K. T., & Champion, P. M. (1995) *J. Phys. Chem. 99*, 3394−3405.

Sage, J. T., & Champion, P. M. (1996) in *Comprehensive Supramolecular Chemistry* (Suslick, K. S., Ed.) Vol. 5, Chapter 8, Pergamon, Oxford, U.K.

Springer, B. A., & Sligar, S. G. (1987) *Proc. Natl. Acad. Sci. U.S.A. 84*, 8961−8965.

Šrajer, V., & Champion, P. M. (1991) *Biochemistry 30*, 7390−7402.

Šrajer, V., Schomacker, K. T., & Champion, P. M. (1986) *Phys. Rev. Lett. 57*, 1267−1270.

Šrajer, V., Reinisch, L., & Champion, P. M. (1988) *J. Am. Chem. Soc. 110*, 6656−6669.

Steinbach, P. J., Ansari, A., Berendzen, J., Braunstein, D., Chu, K., Cowen, B. R., Ehrenstein, D., Frauenfelder, H., Johnson, J. B., Lamb, D. C., Luck, S., Mourant, J. R., Nienhaus, G. U., Ormos, P., Philipp, R., Xie, A., & Young, R. D. (1991) *Biochemistry 30*, 3988−4001.

Tian, W. D., Sage, J. T., Šrajer, V., & Champion, P. M. (1992) *Phys. Rev. Lett. 68*, 408−411.

Tian, W. D., Sage, J. T., & Champion, P. M. (1993) *J. Mol. Biol. 233*, 155−166.

Tian, W. D., Wells, A. V., Champion, P. M., Primo, C. D., Gerber, N., & Sligar, S. G. (1995a) *J. Biol. Chem. 270*, 8673−8679.

Tian, W. D. (1995b) Ph.D. Thesis, Northeastern University, Boston, MA.

Young, R. D., Frauenfelder, H., Johnson, J. B., Lamb, D. C., Nienhaus, G. U., Philipp, R., & Scholl, R. (1991) *Chem. Phys. 158*, 315−327.

Zhu, L., Sage, J. T., Rigos, A. A., Morikis, D., & Champion, P. M. (1992) *J. Mol. Biol. 224*, 207−215.

BI952474U